ANL/GTRI/TM-13/5

Preliminary Accident Analyses for Conversion of the Massachusetts Institute of Technology Reactor (MITR) from Highly Enriched to Low Enriched Uranium

Nuclear Engineering Division

About Argonne National Laboratory

Argonne is a U.S. Department of Energy laboratory managed by UChicago Argonne, LLC under contract DE-AC02-06CH11357. The Laboratory's main facility is outside Chicago, at 9700 South Cass Avenue, Argonne, Illinois, 60439. For information about Argonne and its pioneering science and technology programs, see www.anl.gov.

Availability of This Report

This report is available, at no cost, at http://www.osti.gov/bridge. It is also available on paper to the U.S. Department of Energy and its contractors, for a processing fee, from:

U.S. Department of Energy
Office of Scientific and Technical Information
P.O. Box 62
Oak Ridge, TN 37831-0062
phone (865) 576-8401
fax (865) 576-5728
reports@adonis.osti.gov

Disclaimer

This report was prepared as an account of work sponsored by an agency of the United States Government. Neither the United States Government nor any agency thereof, nor UChicago Argonne, LLC, nor any of their employees or officers, makes any warranty, express or implied, or assumes any legal liability or responsibility for the accuracy, completeness, or usefulness of any information, apparatus, product, or process disclosed, or represents that its use would not infringe privately owned rights. Reference herein to any specific commercial product, process, or service by trade name, trademark, manufacturer, or otherwise, does not necessarily constitute or imply its endorsement, recommendation, or favoring by the United States Government or any agency thereof. The views and opinions of document authors expressed herein do not necessarily state or reflect those of the United States Government or any agency thereof, Argonne National Laboratory, or UChicago Argonne, LLC.

ANL/GTRI/TM-13/5

Preliminary Accident Analyses for Conversion of the Massachusetts Institute of Technology Reactor (MITR) from Highly Enriched to Low Enriched Uranium

prepared by

Floyd E. Dunn, Arne P. Olson, Erik H. Wilson
Nuclear Engineering Division, Argonne National Laboratory

Kaichao Sun, Thomas H. Newton, Jr., and Lin-wen Hu
MIT Nuclear Reactor Laboratory and Nuclear Science and Engineering Department

July 2013

This work is sponsored by the U.S. Department of Energy,
National Nuclear Security Administration Office of Global Threat Reduction (NA-21)

(This page intentionally left blank)

ABSTRACT

The Massachusetts Institute of Technology Reactor (MITR-II) is a research reactor in Cambridge, Massachusetts designed primarily for experiments using neutron beam and in-core irradiation facilities. It delivers a neutron flux comparable to current LWR power reactors in a compact 6 MW core using Highly Enriched Uranium (HEU) fuel.

In the framework of its non-proliferation policies, the international community presently aims to minimize the amount of nuclear material available that could be used for nuclear weapons. In this geopolitical context most research and test reactors, both domestic and international, have started a program of conversion to the use of LEU fuel. A new type of LEU fuel based on an alloy of uranium and molybdenum (U-Mo) is expected to allow the conversion of U.S. domestic high performance reactors like MITR. This report presents the preliminary accident analyses for MITR cores fueled with LEU monolithic U-Mo alloy fuel with 10 wt% Mo. Preliminary results demonstrate adequate performance, including thermal margin to expected safety limits, for the LEU accident scenarios analyzed.

(This page intentionally left blank)

TABLE OF CONTENTS

ABSTRACT ..... **i**

TABLE OF CONTENTS ..... **iii**

TABLE OF FIGURES ..... **v**

LIST OF TABLES ..... **vi**

1.0 INTRODUCTION **1**

2.0 REACTOR GEOMETRY AND CORE POWER DISTRIBUTIONS **2**

2.1 Nominal Element Geometry 3

2.2 Core Power Distributions 4

3.0 PROPERTIES OF MATERIALS **5**

3.1 Thermal properties of Cladding and Structural Components 5

3.2 Fuel Thermal Properties 6

4.0 INSERTION OF EXCESS REACTIVITY **9**

4.1 PARET/ANL Model 9

4.2 Forced Convection Cases 10

4.3 Natural Convection Transients 21

4.4 Concluding Remarks 22

5.0 LOSS OF PRIMARY COOLANT FLOW **24**

5.1 RELAP5 Model 25

5.1.1 Conservative treatment of the peak channels *25*

5.1.2 RELAP5 treatment of fins on the fuel plates *26*

5.2 Initial Conditions and Assumptions 31

5.3 Results 32

5.4 Conclusions 38

6.0 HEAVY WATER AND LIGHT WATER MIXING **39**

6.1 Leakage of Light Water into the Heavy Water Reflector 39

6.2 Leakage of Heavy Water into the Light Water System 40

7.0 MAXIMUM HYPOTHETICAL ACCIDENT **43**

8.0 SUMMARY OF PRELIMINARY ACCIDENT ANALYSES 44

ACKNOWLEDGEMENTS 46

REFERENCES..... 47

TABLE OF FIGURES

Figure 2.1. Layout of the MIT reactor core. 2
Figure 2.2. Axial Power Profiles of Cores with Peak Power Locations. 4
Figure 4.1. HEU, fresh core, 2.3$ in 500 ms: Power, Energy, and Reactivity. 11
Figure 4.2. HEU, fresh core, 2.3$ in 500 ms: Peak Fuel and Clad Temperatures. 12
Figure 4.3. HEU, burned core, 2.3$ in 500 ms: Power, Energy, and Reactivity. 13
Figure 4.4. HEU, burned core, 2.3$ in 500 ms: Peak Fuel and Clad Temperatures. 14
Figure 4.5. LEU, fresh core, 2.3$ in 500 ms: Power, Energy, and Reactivity. 15
Figure 4.6. LEU, fresh core, 2.3$ in 500 ms: Peak Fuel and Clad Temperatures. 16
Figure 4.7. LEU, burned core, 2.3$ in 500 ms: Power, Energy, and Reactivity. 17
Figure 4.8 LEU, burned core, 2.3$ in 500 ms: Peak Fuel and Clad Temperatures. 18
Figure 5.1. Axial Power Profiles of Cores for LOF Analysis. 24
Figure 5.2. Calculated Power and Measured HEU Pump Coastdown Flow. 31
Figure 5.3. Power and Channel Flows for the Fresh HEU LOF. 32
Figure 5.4. Peak End Channel Temperatures for the HEU Fresh Core LOF. 33
Figure 5.5. Peak Interior Channel Temperatures for the HEU Fresh Core LOF. 33
Figure 5.6. Power and Flows for the Fresh LEU LOF. 34
Figure 5.7. Expanded Time Scale for Fresh LEU LOF Power and Flows. 35
Figure 5.8. Peak Temperatures for the Fresh LEU LOF. 35
Figure 5.9. Expanded Time Scale for Peak End Channel Temperatures for Fresh LEU LOF. 36
Figure 5.10, Peak Interior Channel Temperatures for Fresh LEU LOF. 37
Figure 6.1. Effect of light water leakage into the heavy water reflector (HEU case). (a) MCNP results and (b) from the SAR for the MITR. 39
Figure 6.2. Effect of light water leakage into the heavy water reflector (LEU case). 40
Figure 6.3. Effect of heavy water leakage into the light water system (HEU case). (a) MCNP results and (b) from SAR for the MITR. 41
Figure 6.4. Effect of heavy water leakage into the light water system (LEU case). 42

LIST OF TABLES

Table 2.1. HEU and LEU element dimensions. 3
Table 3.1. Modeled Thermal Properties of Aluminum Alloy 6061. 5
Table 3.2. Modeled Thermal Conductivity of Zirconium. 5
Table 3.3. Modeled Volumetric Heat Capacity of Zirconium. 5
Table 3.4. Modeled Volumetric Heat Capacity of HEU UAl_x Fuel. 8
Table 3.5. Modeled Thermal Conductivity of LEU U-10Mo Alloy Fuel. 8
Table 3.6. Modeled Volumetric Heat Capacity of LEU U-10Mo Alloy Fuel. 8
Table 4.1. Timing Event Sequence and Assumptions. 10
Table 4.2. RIA of a 2.3 $ ramp in 500 ms (initial power = 7 MW LEU; 6 MW HEU; 1800 gpm). 11
Table 4.3. RIA of 2.3 $ ramp in 500 ms (initial power = 5 W for LEU and for HEU; 1800 gpm). 19
Table 4.4. RIA of 2.3 $ ramp in 500 ms (initial power = 5 W for LEU and for HEU; 1 mm/s velocity). 19
Table 4.5. RIA of 0.03 dk/k over 60 seconds (initial power = 7 MW for LEU; 6 MW for HEU). 19
Table 4.6. RIA of 0.03 dk/k over 60 seconds (initial power = 5 watts). 20
Table 4.7. RIA of a 1.5 $ step in 1 ms (initial power = 5 W; Tin=44 C; 1 kg/s flow, power trip at 0.1 MW; period trip at 7 s). 20
Table 4.8 Steady-state mass flux at 80 kW ($kg/m^2/s$). 21
Table 4.9. RIA of a 2.3 $ ramp in 500 ms (initial power = 80 kW; natural convection). 22
Table 5.1. MITR Cores Used for LOF Analysis. 24
Table 5.2. Coolant Gap Sizes (Fin Tip-Fin Tip, mil) Used for Peak Channels. 26
Table 5.3. Heat Transfer Parameters for Current Designs 29
Table 5.4. Peak Temperatures, ^oC, for the Loss-of-Flow Accident. 37
Table 7.1 MHA Dose results. 43

1.0 INTRODUCTION

The Massachusetts Institute of Technology Reactor (MITR-II) is a research reactor in Cambridge, Massachusetts designed primarily for experiments using neutron beam and in-core irradiation facilities. It delivers a neutron flux comparable to current LWR power reactors in a compact 6 MW core using Highly Enriched Uranium (HEU) fuel.

In the framework of its non-proliferation policies, the international community presently aims to minimize the amount of nuclear material available that could potentially be diverted for nuclear weapons. In this geopolitical context, most research and test reactors both domestic and international have started a program of conversion to the use of Low Enriched Uranium (LEU) fuel. A new type of LEU fuel based on an alloy of uranium and molybdenum (UMo) is expected to allow the conversion of compact high performance reactors like the MITR-II reactor.

Safety analyses of an MITR core fueled with a monolithic alloy of uranium and 10 wt% molybdenum (U-10Mo) have been conducted to establish the steady state safety basis of the reactor using the feasibility design of the MITR reactor [1.1] [1.2] [1.3]. The thermal hydraulic analyses of the reactor have required detailed power distributions and geometrical considerations in order to identify regions of interest for safety analyses [1.4]. Reference [1.5] contains the feasibility design developed assuming U-7Mo fuel. Calculations for the feasibility design with U-10Mo are described in Reference [1.6], and this design has been used throughout the other works previously referenced.

In order to understand the impacts of accident and transient scenarios in a core fueled with LEU U-10Mo, a set of preliminary accident analyses have been performed. NUREG-1537 guidelines postulate nine classes of accident-initiating scenarios which are addressed in the MITR Safety Analysis Report [1.7, 1.8]. These preliminary analyses include evaluating those expected to be the most challenging to fuel integrity. This work analyzes reactivity insertion accidents, loss of flow pump coast down, heavy and light water mixing, and the maximum hypothetical accident. The objective of these preliminary analyses is to determine the estimated range of conditions and temperatures that the fuel, which is under development, should be expected to experience under off-normal and other transient scenarios.

2.0 REACTOR GEOMETRY AND CORE POWER DISTRIBUTIONS

The MIT Reactor (MITR-II) core is a light water moderated core surrounded by heavy water as a reflector on the sides and below the core. It has a hexagonal design that contains twenty-seven fuel positions in three radial rings (A, B, and C), as shown in Figure 2.1. Typically three of these positions (two in the A-ring and one in the B-ring) are filled with either an in-core experimental facility or a solid aluminum dummy element to reduce power peaking. The remaining positions are filled with standard MITR-II fuel elements.

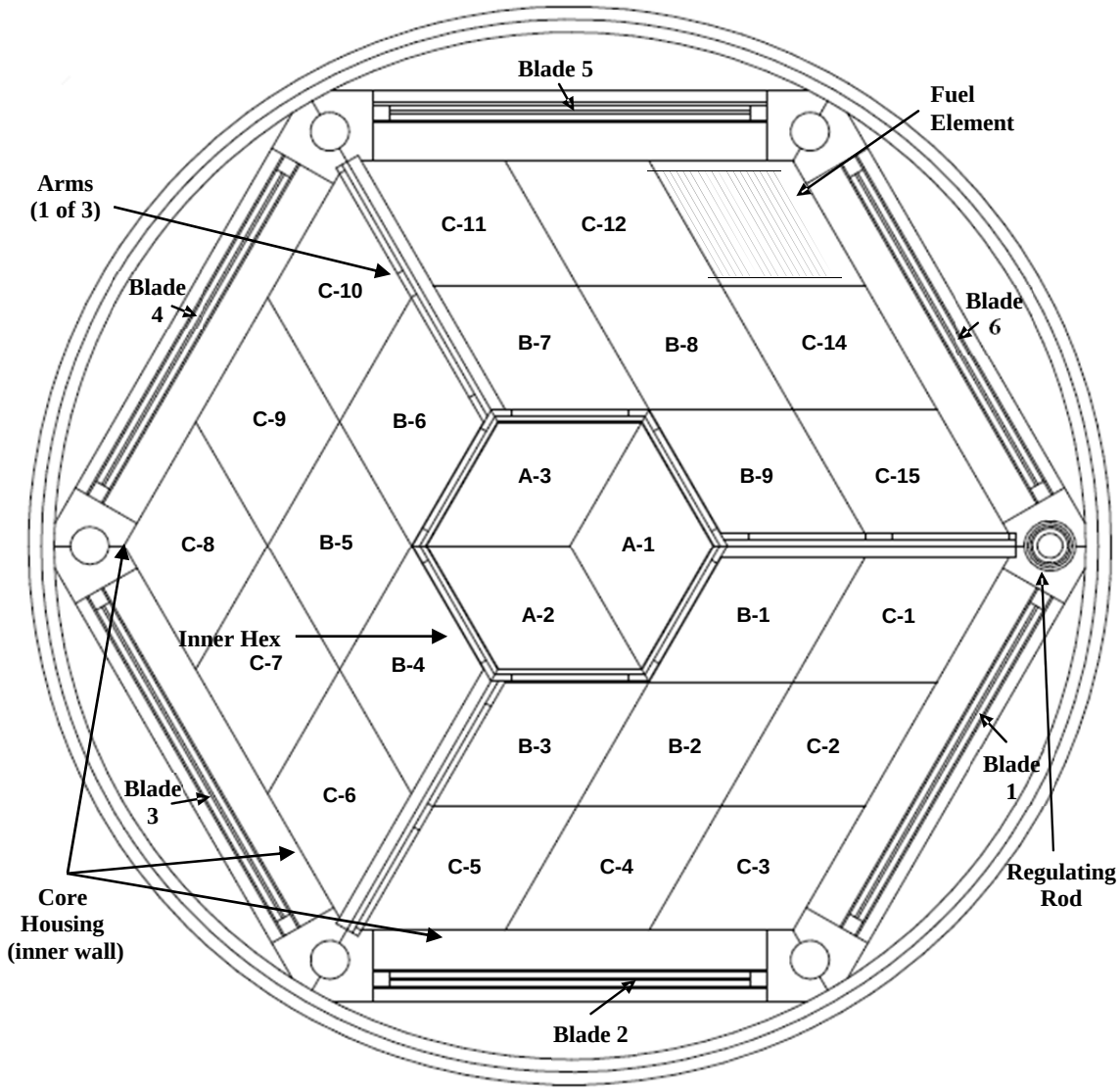

Figure 2.1. Layout of the MIT reactor core.

2.1 Nominal Element Geometry

The proposed LEU design was discussed in [1.1]. Each rhomboid-shaped LEU fuel element contains eighteen aluminum-clad fuel plates with a fuel zone thickness of 0.508 mm (0.020 inch) and fuel zone length of 56.8325 cm (22.375 inch). The LEU fuel modeled is a uranium-molybdenum monolithic alloy enriched up to 19.75% ^{235}U, and with 10 wt% Mo at an overall fuel density of 17.02 g/cm^3. The cladding (consisting of 6061 aluminum alloy and a thin, nominally 0.001 inch thick, zirconium layer at the fuel interface) of each fuel plate is 0.254 mm (0.010 inch) thick. In order to increase heat transfer to the coolant, there are 0.254 mm (0.010 inch) longitudinal fins in addition to the 0.254 mm (0.010 inch) cladding. The thickness of the fuel plate is 1.524 mm (0.060 inch) from fin-tip to fin-tip.

The gaps between fuel plates which form the coolant channels within an element are referred to as interior channels. These interior channels are 1.8288 mm (0.072 inch) from fin-tip to fin-tip. End channels are present on the outside of the outer fuel plates. Table 2.1 compares dimensions of the LEU element to HEU, as described in Reference [1.4]. Note that the dimension mil represents 0.001 inches or 0.0254 millimeters.

Table 2.1. HEU and LEU element dimensions.

Plate and Channel Dimensions	HEU	LEU
Fuel plate length (inch)	23	23
Fuel meat length (inch)	22.375	22.375
Fuel plates per assembly	15	18
Interior (full) channels per assembly	14	17
End (partial) channels per assembly	2	2
Fuel meat thickness (mil)	30	20
Fuel meat width (inch)[a]	2.082	2.082
Clad thickness (base of fin to fuel surface)	15 (6061 Al)	10 (6061Al + Zr)
Plate to plate pitch, CL to CL (mil)	158	132
Interior channel water gap (fin tip-to-tip) (mil)	78	72
Effective interior channel thickness (mil)	88	82
Finned width (inch)[a]	2.2	2.2
Number of fins per plate	110 per side	110 per side
Fin depth (mil)	10	10
Fin width (mil)	10	10
Width between fuel meat and side plate (mil)	113	113
Width between fins and side plate (mil)	54	54
Channel width (inch)[a]	2.308	2.308
Side plate thickness (mil)	188	188
Side plate flat-to-flat, outer edge of one side plate to outer edge of second side plate on element (inch)	2.375	2.375
Element end flat-to-flat (inch)	2.380	2.380
Outer plate fin-tip to side plate end plane (mil)	44	38
Effective outer plate gap to side plate end plane (mil)	49	43
Outer plate fin-tip to nozzle at full width (mil)[b]	56.5	50.5
Effective outer plate gap to nozzle at full width (mil)	61.5	55.5
Outer plate fin-tip to nozzle at full width (mil)	56.5	50.5

[a] For thermal hydraulic analysis, channel width is the fuel meat width of 2.082 inch (0.052883 m) due to treatment in accounting for conductive cooling using the 2.308 channel width.

[b] Since element is closed only on two side, the distance from the plate surface to the end fitting nozzle defines the end channel nominal dimension (LEU 50.5 mil) [1.4].

2.2 Core Power Distributions

Power distributions were previously calculated Reference in [1.4]. For a given HEU or LEU core, a fuel plate stripe approach was used. Four stripes running lengthwise were used for each fuel plate in the core, with 18 axial nodes in each stripe. Neutronics calculations were made to determine the power in each axial node of each stripe for each plate of each element in the core. The all-fresh cores had the maximum locations of power from a series of cores representing MITR fuel management. All-fresh cores, as well as the depleted cores, with locations of maximum power, are shown in Figure 2.2. These were selected for preliminary accident analyses since the peak power locations are anticipated to yield limiting temperatures, although additional core states should be included in the next phase of analyses due to the effects of depletion and oxide formation on the plate surface.

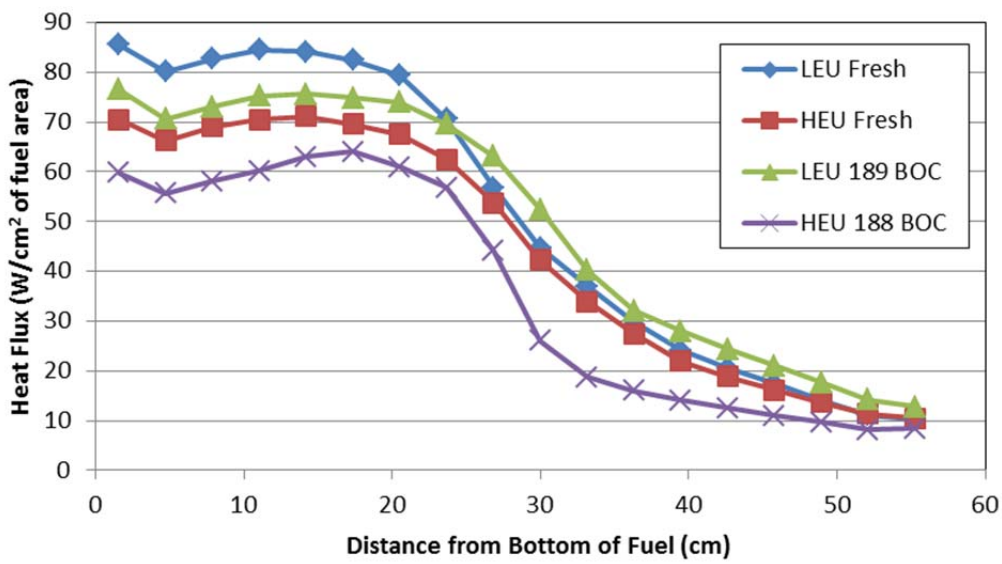

Figure 2.2. Axial Power Profiles of Cores with Peak Power Locations.

3.0 PROPERTIES OF MATERIALS

Thermal properties used in modeling reactivity insertion and loss of flow events are listed in this section.

3.1 Thermal properties of Cladding and Structural Components

Thermal properties of the Aluminum Alloy 6061 were modeled as listed in Table 3.1 [3.1]. This reference was also used as a basis of many of other references for materials properties. Zirconium thermal conductivity, k, in W/m-K is based on Reference [3.2]:

$$k = 8.8527 + 7.0820 \times 10^{-3}\ T + 2.5329 \times 10^{-6}\ T^2 + 2.9918 \times 10^3\ T^{-1} \qquad (3.1)$$

where the temperature in K is 298 K ≤ T ≤ 2000 K. Also based on this reference is the zirconium heat capacity, C_p, in J/mol-K:

$$C_p = 24.1618 + 8.75582 \times 10^{-3}\ T - 69942\ T^{-2} \qquad (3.2)$$

where the temperature in K is 298 K ≤ T ≤ 2000 K. Modeled zirconium thermal properties are listed in Tables 3.2 and 3.3.

Table 3.1. Modeled Thermal Properties of Aluminum Alloy 6061.

Temperature (ºC)	Thermal Conductivity (W/m-K)	Volumetric Heat Capacity (MJ/m^3-K)
20	167.5	2.539
260	184.3	2.688
537.8	201.1	2.828
1648.9	268.1	3.391

Table 3.2. Modeled Thermal Conductivity of Zirconium.

Temperature (ºC)	Thermal Conductivity (W/m-K)
20	21.35
93.3	19.95
204.4	19.08
277.4	18.96
371.1	19.11

Table 3.3. Modeled Volumetric Heat Capacity of Zirconium.

Temperature (ºC)	Volumetric Heat Capacity (MJ/m^3-K)
20	1.866
204.4	2.019
537.8	2.244

Where oxide on the surface of the cladding was modeled, a thermal conductivity value of 2.25 W/m-K was used [3.3]. The oxide volumetric heat capacity was also assumed to be constant with temperature, and was modeled as 3.12 MJ/m^3-K [3.4].

3.2 Fuel Thermal Properties

The value of thermal conductivity for the HEU fuel meat was assumed to be 40 W/m-K [3.5]. This value is conservative given the range listed in Figure 8 of this reference, where the thermal conductivity depends strongly on the volume fraction of the dispersed fuel (33.5%) plus porosity of the fuel (7%) which equals 40.5% as derived from materials defined in Reference [1.1]. Table 3.4 lists the modeled HEU fuel heat capacity [3.1].

For U-10Mo alloy, the thermal conductivity, k, in W/m-°C is given by Burkes et. al. using the nominal values as:

$$k = 10.2 + 3.51 \times 10^{-2}\ T \qquad (3.3)$$

where the temperature in °C is 20°C ≤ T ≤ 800°C [3.6]. This reference also gives nominal heat capacity, C_p, in J/g-C as:

$$C_p = 0.137 + 5.12 \times 10^{-5}\ T + 1.99 \times 10^{-8}\ T^2 \qquad (3.4)$$

where the temperature in °C is 100°C ≤ T ≤ 1000°C.

The density of the fresh fuel was assumed to be 17.02 g/cm^3 when calculating the volumetric heat capacity. This density corresponds to an approximate 99% dense LEU U-10Mo [1.1]. Reference [3.6] proposes for the density of LEU U-10Mo, $\rho_{LEU\text{-}10Mo}$, in g/cm^3:

$$\rho_{LEU\text{-}10Mo} = 17.15 - (8.63 \times 10^{-4} \pm 2.77 \times 10^{-5})(T + 20) \qquad (3.5)$$

where the temperature in °C is 20°C ≤ T ≤ 700°C. However the density would then be 17.15 g/cm^3 at -20°C whereas the author states that the theoretical density of LEU U-10Mo is 17.15 g/cm^3. Equation 5 appears to be a misprint which would be corrected by changing (T + 20) to (T – 20) which gives:

$$\rho_{LEU\text{-}10Mo} = 17.15 - (8.63 \times 10^{-4} \pm 2.77 \times 10^{-5})(T - 20) \qquad (3.6)$$

where the temperature in °C is 20°C ≤ T ≤ 700°C. Modeling density as 17.02 g/cm^3 is thus consistent with referenced data assuming as-fabricated porosity of approximately 1%.

Thermal conductivity of fuel is degraded by the presence of voids whether due to porosity or fission gas bubbles. However, thermal conductivity as shown in Eqn. 3.3 has already been corrected for porosity by the authors of Reference [3.6]. Hence Eqn. 3.3, which represents the fully dense value, is in this work modified by the reduction in thermal conductivity due to porosity assumed in the fresh fuel. Likewise irradiated fuel thermal conductivity is reduced due to fission gas bubbles as follows. Various treatments have been proposed in order to model a calculated reduction in thermal conductivity due to inhomogeneous materials containing both solids and pores. Peddicord [3.7], like other methods [3.8, 3.9, 3.10, 3.11], represent pores as a fraction of a material that contributes a small or negligible amount to the

thermal conductivity, and assumes a regular homogeneous arrangement of pores in the solid. In Reference [3.6], Peddicord fit the fractional reduction in thermal conductivity, $F_{k\text{-reduction}}$, using:

$$F_{k\text{-reduction}} = e^{-2.14p} \tag{3.7}$$

which is applicable for pore fractions, p, in the range of $0 \leq p \leq 0.3$. This range is applicable to MITR fresh and depleted cores where for fresh fuel, the 1% assumed pore fraction gives $F_{k\text{-reduction}} = 0.98$ according to Eqn. 3.7. For depleted cores the swelling due to fission gas bubbles, $(\Delta V/V_o)_g$, can be calculated as per Kim and Hoffman [3.12]:

$$(\Delta V/V_o)_g = 1.0 f_d, \quad \text{for} \quad f_d \leq 3 \times 10^{21} \tag{3.8}$$

$$(\Delta V/V_o)_g = 3.0 + 2.3(f_d - 3) + 0.33(f_d - 3)^2, \text{ for } \quad f_d > 3 \times 10^{21} \tag{3.9}$$

where f_d is fission density in 10^{21} cm^{-3}. Note $(\Delta V/V_o)_g$ is not fractional but is given in units of percent. This uses the original volume, V_o , and the change in volume ΔV. For MITR, maximum local ^{235}U burnup during the core cycle when maximum power occurs is 1.2×10^{21} cm^{-3} [3.13]. However, in order to conservatively reduce the thermal conductivity, this work uses the maximum local burnup expected in all cores to calculate $F_{k\text{-reduction}}$. Reference [3.13] lists for representative MITR fuel management predicted maximum local burnup of 5.2×10^{21} cm^{-3}.

The final fuel swelling due to both fission product solids and gas swelling should be used to calculate the pore fraction, p, particularly since a larger fraction of the swelling here arises from solid fission products. In order to calculate p, Reference [3.14] Equation 3 is repeated here as Eqn. 3.10.

$$p = (1/100)\,(\Delta V/V_o)_g \,/\, [1 + (\Delta V/V_o)_f] \tag{3.10}$$

Note that $100 + (\Delta V/V_o)_f$ gives the final fuel swelling (in percent) and thus the present authors correct Eqn. 3.10 as:

$$p = (\Delta V/V_o)_g \,/\, [100 + (\Delta V/V_o)_f] \tag{3.11}$$

where $(\Delta V/V_o)_f$ is in percent and is calculated from Reference [3.12] as:

$$(\Delta V/V_o)_f = 5.0 f_d, \quad \text{for} \quad f_d \leq 3 \times 10^{21} \tag{3.12}$$

$$(\Delta V/V_o)_f = 15 + 6.3(f_d - 3) + 0.33(f_d - 3)^2, \text{ for } \quad f_d > 3 \times 10^{21} \tag{3.13}$$

where $(\Delta V/V_o)_f$ is overall fuel swelling due to both fission product solids and gas. The pore fraction in the irradiated fuel is thus estimated to be 7% giving $F_{k\text{-reduction}} = 0.85$. This treatment remains conservative since power was not reduced despite the use of maximum ^{235}U burnup. Table 3.5 lists the modeled thermal conductivity of fresh unirradiated and irradiated LEU fuel where Eqn. 3.3 is reduced by the $F_{k\text{-reduction}}$ for fresh (0.98) and irradiated fuel (0.85). Table 3.6 lists the modeled heat capacity of the LEU fuel [3.1]. While different than Eqn. 3.4, the values of the fuel heat capacity in Table 3.6 are deemed acceptable for preliminary analysis, and subsequent analyses should assess the impact of variations in thermophysical properties.

Table 3.4. Modeled Volumetric Heat Capacity of HEU UAl_x Fuel.

Temperature (ºC)	Volumetric Heat Capacity (MJ/m^3-K)
20	2.247
260	2.388
537.8	2.560
1648.9	3.250

Table 3.5. Modeled Thermal Conductivity of LEU U-10Mo Alloy Fuel.

Temperature (ºC)	Unirradiated Thermal Conductivity (W/m-K)	Irradiated Thermal Conductivity (W/m-K)
20	10.64	9.30
800	37.36	32.67

Table 3.6. Modeled Volumetric Heat Capacity of LEU U-10Mo Alloy Fuel.

Temperature (ºC)	Volumetric Heat Capacity (MJ/m^3-K)
20	2.362
93.3	2.430
204.4	2.538
315.6	2.655
426.7	2.781

4.0 INSERTION OF EXCESS REACTIVITY

4.1 PARET/ANL Model

As a general principle, during rapid power excursion transients a reactor can handle power bursts that are much higher than the steady-state burnout power level, since these power bursts last only for a few tenths of a second and the burnout heat flux can be substantially higher than steady-state if the period is less than 1 second [4.1, 4.2]. It is only during steady-state operation or slow transients at power levels above the safety limit curves that melting of the fuel plate may result from a boiling "crisis" such as Departure from Nucleate Boiling or Flow Instability. To cause fuel damage during a rapid transient, the product of power level and time must yield enough total energy to reach the melting temperature of a fuel plate. Such reactor behavior has been conclusively shown by hundreds of power excursion tests performed at the Special Power Excursion Reactor Test (SPERT) facility at the National Reactor Testing Station in Idaho [4.3]. Reactivity Insertion Accident Analysis (RIA) was performed using PARET/ANL Version 7.5, with all calculations performed in double precision.

The reactor cores of interest contain either HEU UAl_x with 15 plates and fins, or LEU finned U-10Mo, with 18 plates. The effect of fins on heat transfer rates is accounted for by scaling them by a fin effectiveness factor of 1.90 for HEU and 1.89 for LEU. For Reynolds numbers between 10,000 and 100,000, the friction loss coefficient for the fins is 0.195 for HEU and 0.1948 for LEU. Burned cores are also analyzed. The reactor model in PARET is approximated as being represented by two channels, the first of which represents the channel with locations of maximum power, as shown in Section 2.2, and the second is the remainder of the core. That channel is almost the average channel. It provides most of the reactivity feedback from changes in temperature of fuel and coolant. Point-kinetics parameters of β_{eff} and l_p vary with the core of interest. Each core has unique axial power shapes and peaking factors, and unique feedback coefficients from the Doppler effect in the fuel meat, from void/density change in the coolant, and from temperature change in the coolant.

The total worth of the control blades differ for the HEU vs. LEU cores. It is assumed that the delay time between scram signal and blade motion is 0.10 second. Also assumed is that the blade insertion rate is 0.4741 m/s, which achieves 80 % insertion within 1.0 seconds for a full-insertion stroke of 0.5334 m. All blade reactivity worths are assumed to be linear between full-in and 12 inches-out. All calculations assume that the blades are banked at 12 inches (0.3048 m).

The blade worths from 12 inches withdrawn to fully inserted are:

1. HEU, Fresh -8.10$
2. HEU, Burned -8.56$
3. LEU, Fresh -6.38$
4. LEU, Burned -6.98$

The events analyzed are:

1. Ramp insertion over 500 ms of 2.3 $ with control blades initially banked at 0.3048 m
    a. Fresh fuel
    b. Burned fuel
2. Long, slow ramp insertion of 0.03 dk/k over 60 seconds ($5x10^{-4}$ dk/k/s) with control blades initially banked at 0.3048 m
    a. Fresh fuel
    b. Burned fuel

Coolant volumetric flow rates are set to 1800 gpm for full-flow conditions. The cores containing fresh fuel have 22 fuel assemblies, while the "burned" cores contain 24 fuel assemblies. The control blade and regulating rod speeds are designed to limit the reactivity addition rate to less than $5x10^{-4}$ dk/k/s. This is the basis for event type 2. It bounds possible ramp rates caused by motion of the control blades or regulating rod.

Shim blade control element and control system timing assumptions used for RIA accident analysis can be represented as a sequence of events in time following a scram signal at arbitrary time zero. Table 4.1 shows that time sequence.

Table 4.1. Timing Event Sequence and Assumptions.

Event	Cumulative time after scram setpoint (sec)
RIA event begins	
Scram setpoint reached	0
Delay before blades begin to move	0.1
Blades inserted 80% (start at 12 inch)	0.38
Blades inserted 100% (start at 12 inch)	0.45

There is no credible mechanism for a reactivity ramp insertion of this magnitude in less than 1 second. To be conservative, the analysis assumes that the reactivity insertion takes place as a linear ramp over 500 ms, and is held constant at 2.3 $ after 500 ms. These events are assumed to begin at either very low power (5 watts) or at full power of 6 MW for HEU or 7 MW for LEU. All safety systems are functional. The power trip set point is at 120% power, and the period trip set point is at a minimum period of 7 seconds. The coolant inlet temperature is 44 ºC, and the mass flow rate is assumed to be 1800 gpm through the heated channels at full power. Five watt operation was calculated for flows of 1800 gpm and 1 mm/sec flow velocity.

Reported are temperatures for limiting accident and transient cases and other criteria of safety used in the HEU safety basis. Temperatures: at the fuel meat centerline are reported, as well as at the interface between the clad and the meat (HEU), or at the interface between the zirconium interlayer and the aluminum portion of the cladding (LEU).

4.2 Forced Convection Cases

Table 4.2 lists key results for a series of reactivity insertion accidents caused by a fast ramp extending over 500 ms, for 2.3 $ insertion. This insertion is linear over 500 ms. It is held constant once it is fully inserted. The control blades are always actuated almost immediately by the period trip, once the reactivity ramp begins. The power trip would happen later in time should the period trip not function. It is noteworthy that the minimum burnout ratio shown is always >1.0, indicating no burnout conditions ever occurred in that case.

Figures 4.1 through 4.8 show key results of power, energy release, reactivity, peak fuel temperature, and peak clad temperature for the transients listed in Table 4.2.

Table 4.2. RIA of a 2.3 $ ramp in 500 ms (initial power = 7 MW LEU; 6 MW HEU; 1800 gpm).

Core Description	Peak Fuel Centerline Temperature (°C)	Peak Clad Temperature (°C)	Peak Power (MW)	Min. Burn-out Ratio	Trip	Time Step (s)
HEU, Fresh	85.6	81.3	10.85	6.06	Period	1.E-6
HEU, Burned	83.5	79.6	10.89	6.51	Period	1.E-6
LEU, Fresh	104.2	91.5	12.40	4.48	Period	1.E-6
LEU, Burned	102.1	90.3	12.45	4.85	Period	1.E-6

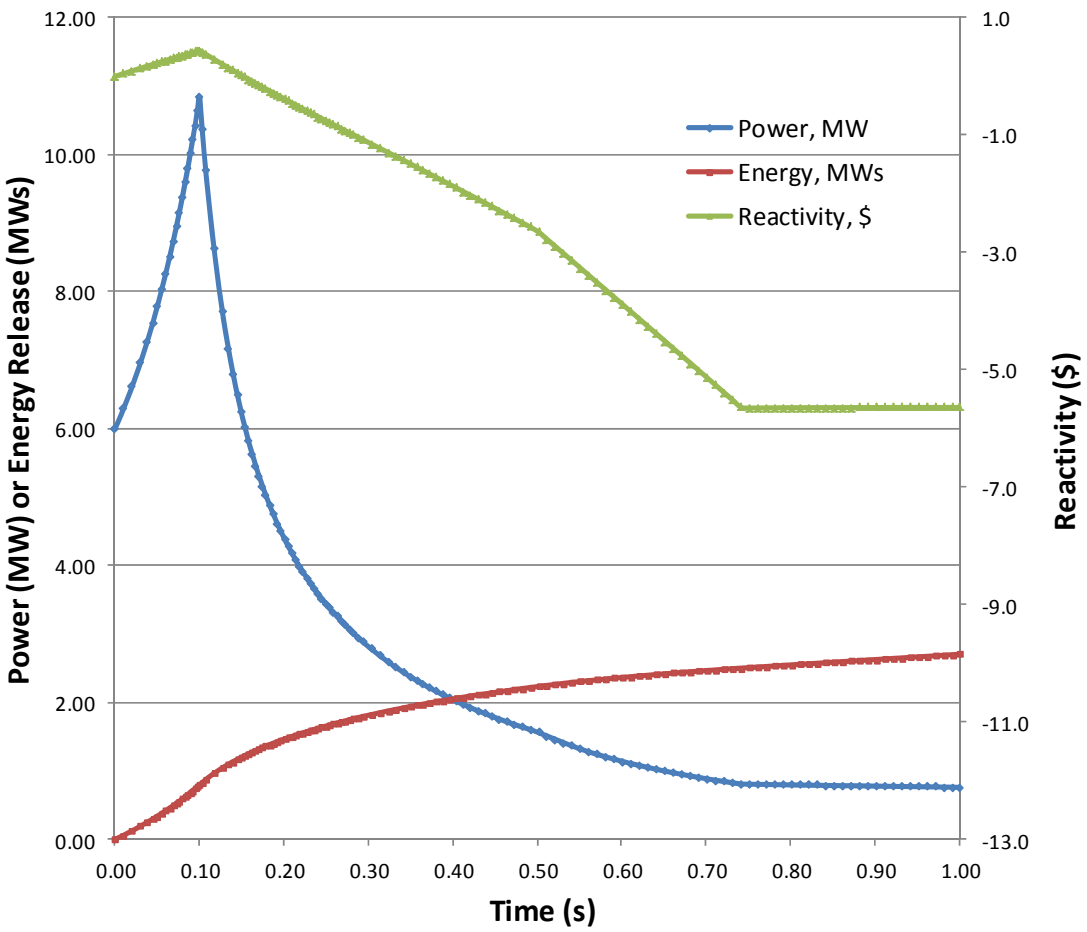

Figure 4.1. HEU, fresh core, 2.3$ in 500 ms: Power, Energy, and Reactivity.

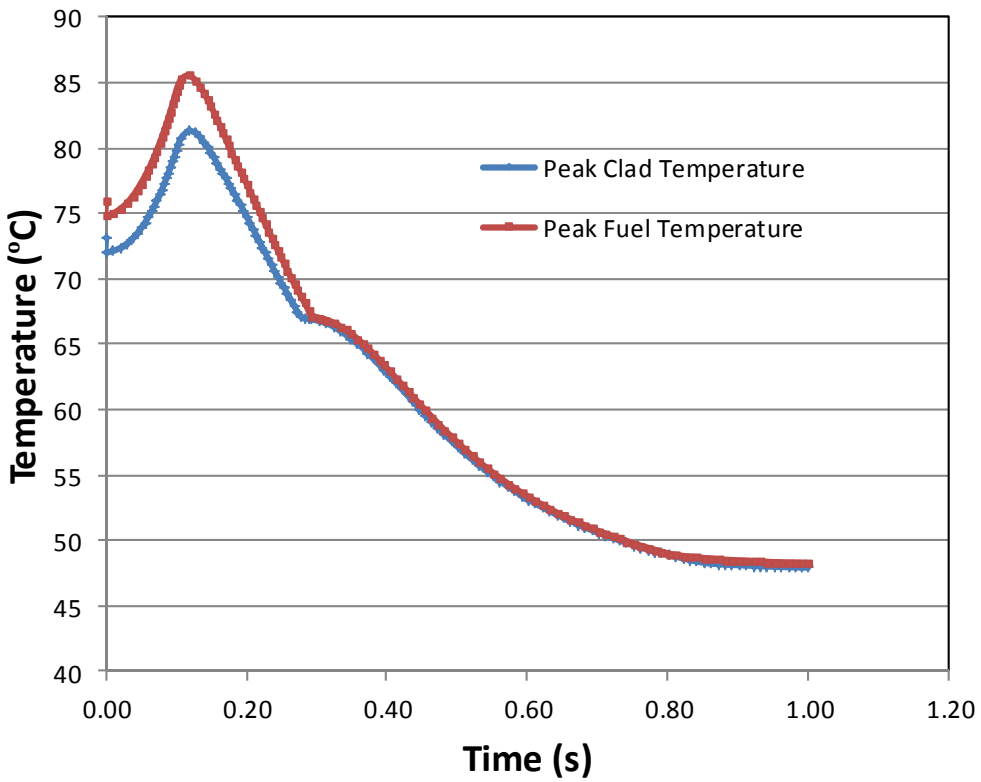

Figure 4.2. HEU, fresh core, 2.3$ in 500 ms: Peak Fuel and Clad Temperatures.

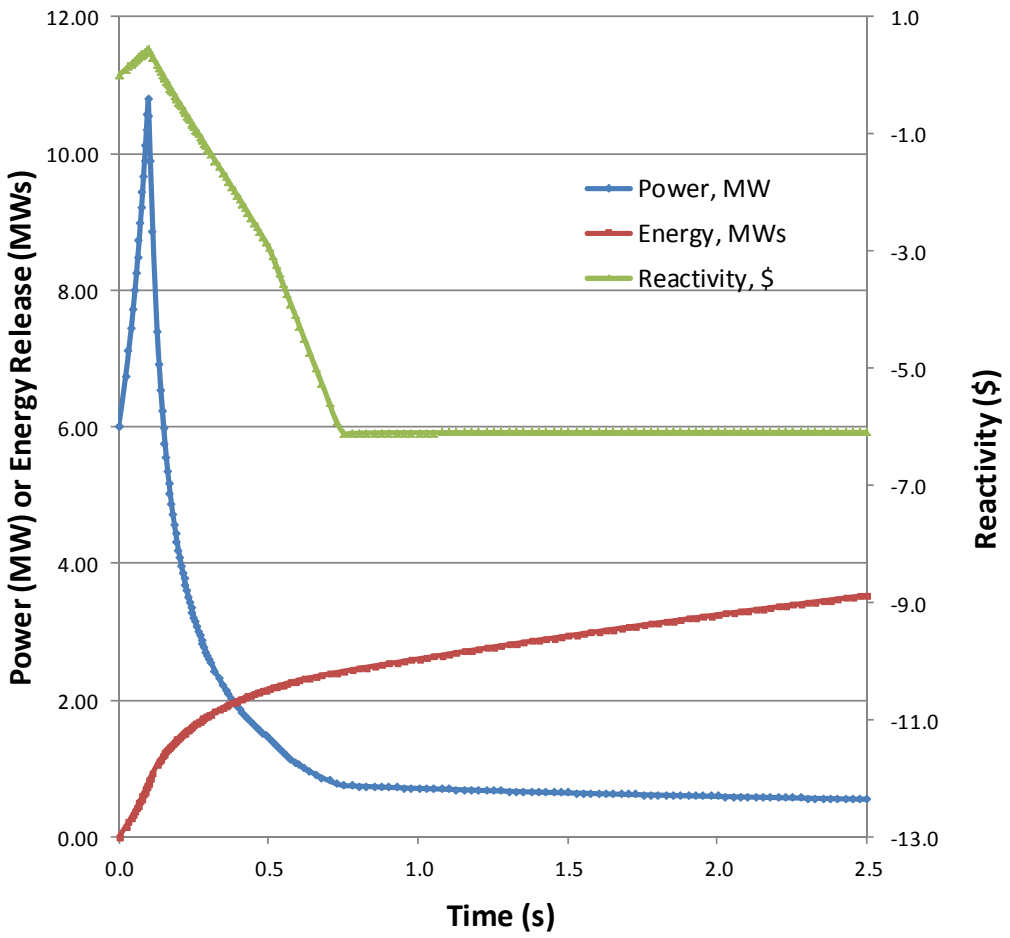

Figure 4.3. HEU, burned core, 2.3$ in 500 ms: Power, Energy, and Reactivity.

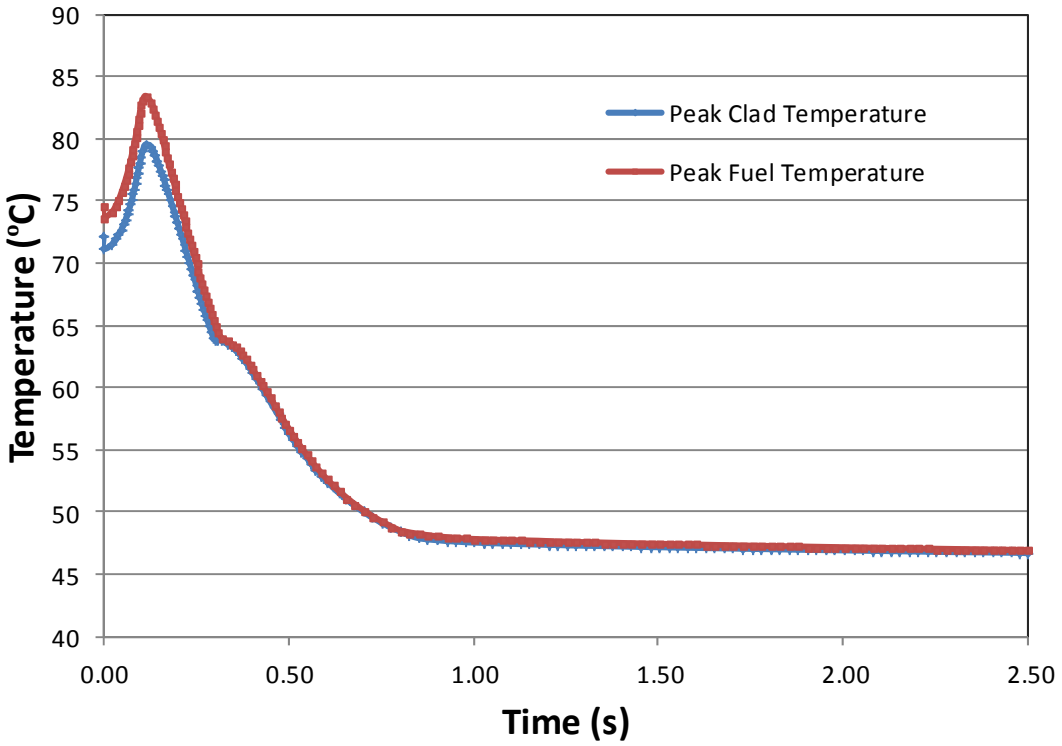

Figure 4.4. HEU, burned core, 2.3$ in 500 ms: Peak Fuel and Clad Temperatures.

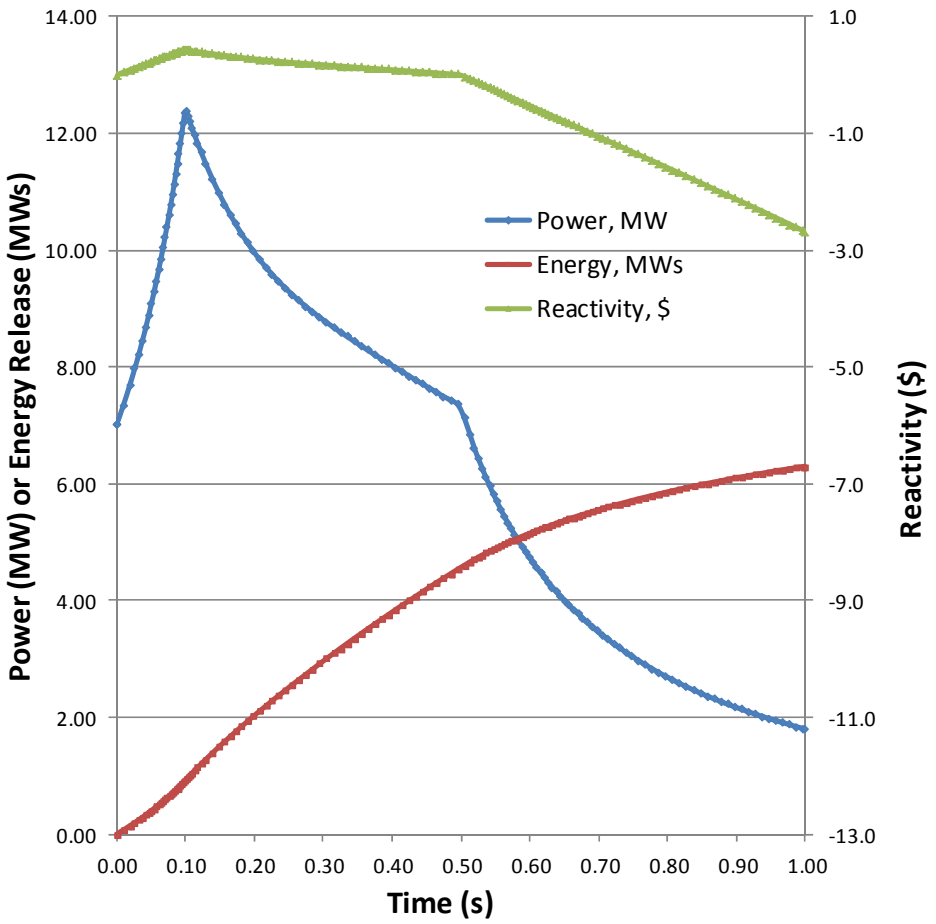

Figure 4.5. LEU, fresh core, 2.3$ in 500 ms: Power, Energy, and Reactivity.

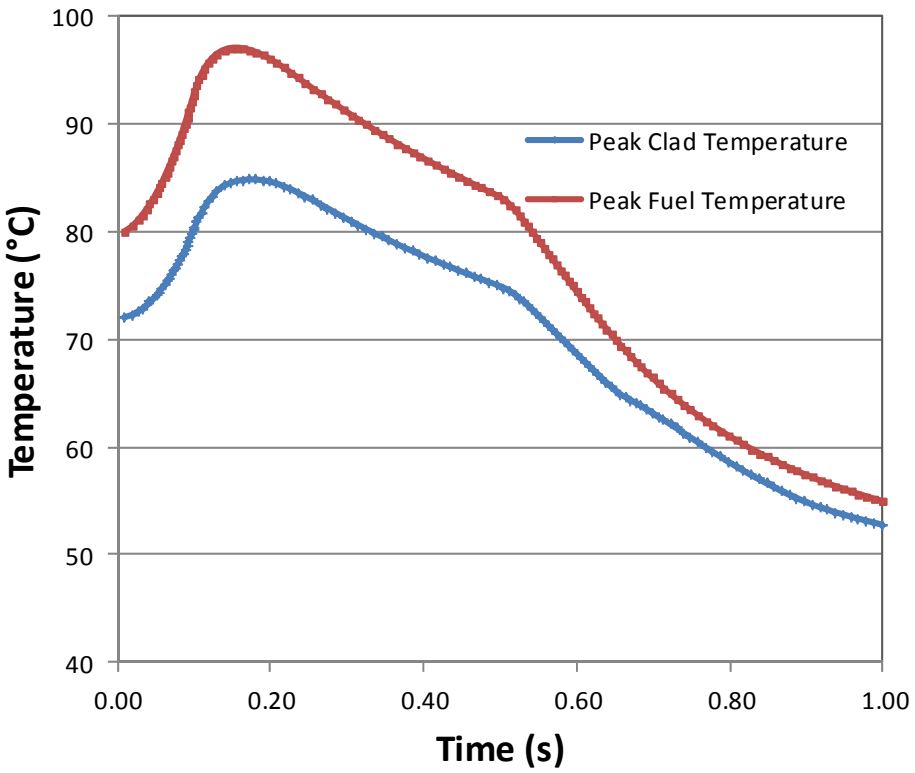

Figure 4.6. LEU, fresh core, 2.3$ in 500 ms: Peak Fuel and Clad Temperatures.

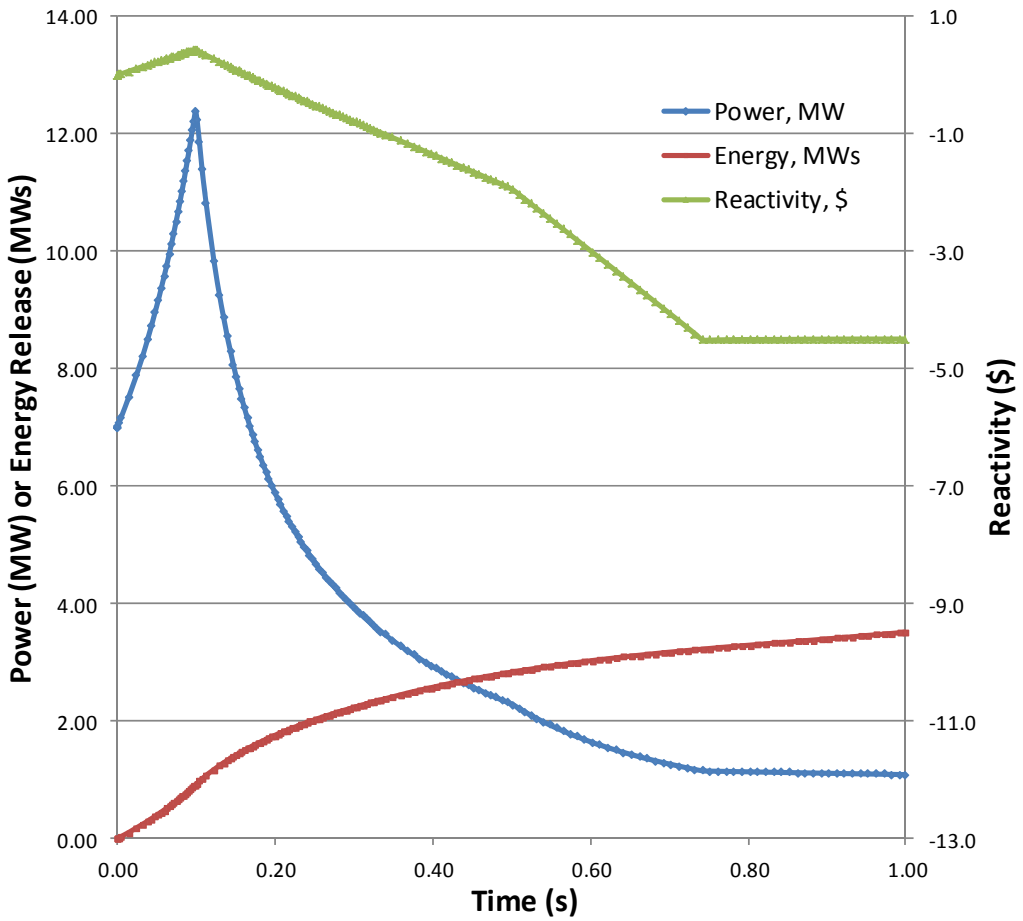

Figure 4.7. LEU, burned core, 2.3$ in 500 ms: Power, Energy, and Reactivity.

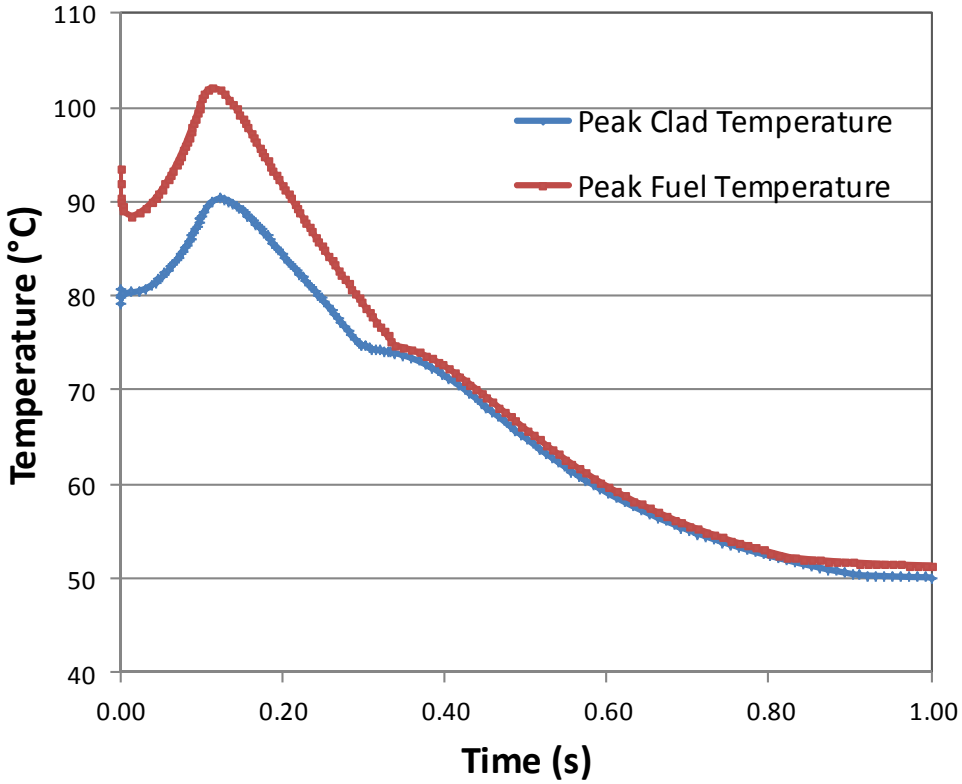

Figure 4.8. LEU, burned core, 2.3$ in 500 ms: Peak Fuel and Clad Temperatures.

The results shown in Table 4.3 are for the same reactor conditions as in Table 4.2, except that the initial power is always 5 watts. All cases listed in Table 4.3 and Table 4.4 undergo a period trip immediately upon initiation of the reactivity ramp. At that moment, the actual period is about 0.1 second. The minimum burnout ratio in all cases is very large, because there is no significant power or energy release by these events. The results shown in Table 4.4 are for the same reactor conditions as in Table 4.3, except Table 4.4 does not have a forced flow condition since substantial power is required to establish natural convection as discussed in the next section. These events are not shown in figures because they are in essence non-events.

Table 4.3. RIA of 2.3 $ ramp in 500 ms (initial power = 5 W for LEU and for HEU; 1800 gpm).

Core Description	Peak Fuel Centerline Temperature (°C)	Peak Clad Temperature (°C)	Peak Power (MW)	Min. Burn-out Ratio	Trip Activated First	Time Step (s)
HEU, Fresh	44.00	44.00	9.38E-6	7.2E+6	Period	1E-6
HEU, Burned	44.00	44.00	9.38E-6	8.3E+6	Period	1E-6
LEU, Fresh	44.00	44.00	9.38E-6	6.1E+6	Period	1E-6
LEU, Burned	44.00	44.00	9.38E-6	6.7E+6	Period	1E-6

Table 4.4. RIA of 2.3 $ ramp in 500 ms (initial power = 5 W for LEU and for HEU; 1 mm/s velocity).

Core Description	Peak Fuel Centerline Temperature (°C)	Peak Clad Temperature (°C)	Peak Power (MW)	Min. Burn-out Ratio	Trip Activated First	Time Step (s)
HEU, Fresh	44.04	44.04	9.38E-6	1.7E+5	Period	1E-6
HEU, Burned	44.04	44.04	9.38E-6	2.1E+5	Period	1E-6
LEU, Fresh	44.04	44.04	9.38E-6	1.7E+5	Period	1E-6
LEU, Burned	44.04	44.04	9.38E-6	1.9E+5	Period	1E-6

Tables 4.5 and 4.6 provide predicted consequences for a long, slow ramp set up to keep the period above 7 seconds for some time, until the power trip is actuated. The only difference between Table 4.5 and Table 4.6 is the reactor power at the initial condition.

Table 4.5. RIA of 0.03 dk/k over 60 seconds (initial power = 7 MW for LEU; 6 MW for HEU).

Core Description	Peak Fuel Centerline Temperature (°C)	Peak Clad Temperature (°C)	Peak Power (MW)	Min. Burnout Ratio	Trip Initiator and time (s)	Time Step (s)
HEU, Fresh	80.6	77.2	7.262	7.26	Power, 3.49	1.E-4
HEU, Burned	79.1	76.1	7.263	7.69	Power, 3.49	1.E-4
LEU, Fresh	95.9	85.5	8.470	5.49	Power, 2.53	1.E-4
LEU, Burned	107.2	85.5	8.473	5.90	Period, 2.31	1.E-4

Table 4.5 indicates that the reactivity insertion rate is just a little too high for the first three cases, when compared to the 4th row (LEU, Burned). Notice that the trip was on period less than 7 seconds for the first three cases, and on power for the last one.

Table 4.6. RIA of 0.03 dk/k over 60 seconds (initial power = 5 watts).

Core Description	Peak Fuel Centerline Temperature (°C)	Peak Clad Temperature (°C)	Peak Power (MW)	Min. Burnout Ratio	Trip Initiator and time (s)	Time Step (s)
HEU, Fresh	44.00	44.00	7.04E-6	7.7E+6	Period, 3.16	1.E-4
HEU, Burned	44.00	44.00	7.04E-6	8.3E+6	Period, 3.16	1.E-4
LEU, Fresh	44.00	44.00	7.00E-6	6.7E+6	Period, 3.10	1.E-4
LEU, Burned	44.00	44.00	6.84E-6	7.40E+6	Period, 2.83	1.E-4

The SAR [1.7] identified the most limiting case for a step insertion to be one initiated at low power and at low coolant flow. It was noted that this initiating condition would delay control system response. But that conclusion required the (unstated) assumption that the period trip was disabled. The present analyses show that any event involving reactivity insertion leads immediately to a period trip. Table 4.7 provides results which show that an extremely steep ramp—effectively a step—causes only a small rise in peak fuel or clad temperature, provided that the period trip is functional.

Table 4.7. RIA of a 1.5 $ step in 1 ms (initial power = 5 W; Tin=44 ºC; 1 kg/s flow, power trip at 0.1 MW; period trip at 7 s).

Core Description	Peak Fuel Centerline Temp. (°C)	Peak Clad Temp. (°C)	Peak Power (MW)	Min. Burn-out Ratio	Trip	Time Step (s)
HEU, Fresh	44.05	44.05	0.00622	8660	Period	1.E-6
HEU, Burned	44.05	44.05	0.00929		Period	1.E-6
LEU, Fresh	44.18	44.15	0.0429		Period	1.E-6
LEU, Burned	44.19	44.16	0.0465		Period	1.E-6

4.3 Natural Convection Transients

Steady-state natural convection mass flow rates are first established by running the PARET code in "power-level-specified" mode. The point-kinetics equations are not solved when in this mode. Instead, power versus time is specified at some constant value for the duration of the problem. The code is run sufficiently long to show that the mass fluxes (kg/m^2/s) in each channel have attained steady-state values. The next step is to go back to "reactivity-specified mode" and set up a calculation that will be reactivity-driven, which will use information about the converged steady-state mass flow rates from the first step. For the present two channel model, one can set the mass flux for the reactor to the converged value for the "average" channel. It was found that the mass fluxes converged well after about 40-50 seconds. The values reached at 60 seconds were taken to be the ultimate converged values. In the second step, the mass flux for the average channel is assigned to all channels, as the initial condition at time t=0. Then this calculation can immediately proceed with the transient event. It is important to note that this approach conservatively sets the mass flux, because the initial (time=0) mass flux in the hot channel is less than its steady-state value. Once the event begins, the flow solution adjusts and the mass flux in the hot channel increases in order to match the pressure drop over the core.

Table 4.8 shows the mass flux values predicted for steady-state operation at 80 kW, with the coolant inlet temperature at 44 ºC, for various cores. The PARET code was run using the option which selects the Sellars correlation (Nu=4.36). The Elenbaas correlation was also used and found to yield steady-state mass fluxes that were 0.2% lower than those obtained by the Sellars correlation. PARET has a third option for natural convection which has always been in the code. But it must be adjusted to fit a given reactor situation. The user can select his choices for parameters HTTCON and HTTEXP. The Elenbaas and Sellars correlations require no such adjustment. All values reported in Tables 4.10 and 4.11 used the Sellars correlation because it was most conservative regarding predicting peak temperatures. The values obtained for channel 2 differ primarily because the total coolant flow areas differ between HEU and LEU cores. Relative power production also has an effect on the mass fluxes, which shows up most clearly in the values obtained for the hot channels. The burned channels consistently have power distributions which are slightly flattened when compared with fresh channels. Consequently they have slightly reduced mass flux when compared with fresh channels.

Table 4.8 Steady-state mass flux at 80 kW (kg/m^2/s).

Channel	HEU	HEU-burned	LEU	LEU-burned
1 (hot)	77.58	72.79	71.84	70.63
2 (average)	62.98	62.94	52.65	50.26

The mass fluxes for steady-state shown in Table 4.8 were used as initial conditions for an RIA consisting of a 2.3$ ramp in 500 ms. Table 4.9 shows the results for this RIA. In every case, the period trip occurs almost instantaneously as the reactivity ramp begins. Then the 0.10 second delay takes place before control rod insertion begins. The result is that the power peaks at 0.10001 second in all 4 cases. The energy release at time of peak power is essentially the same at 0.01072 MWs for HEU, and 0.01075 MWs for LEU. This energy release is very small. The hot channel mass flux immediately starts to increase, which causes the peak temperature to drop, while the power initially rises because of the reactivity ramp. These effects essentially cancel out. Had the event been modeled with the steady-state mass flux in the hot channel, then the peak fuel and clad temperatures would have been smaller. As an example, the steady-state peak fuel and clad temperatures for HEU, Fresh, were 53.94 ºC and 53.91 ºC. The steady-state channel exit temperatures for HEU, Fresh, were 52.75 ºC and 51.34 ºC, respectively.

It is concluded that an RIA consisting of a 2.3 $ ramp in 500 ms, starting in steady-state at 80 kW and with natural-convection flow, leads to very little energy release, which in turn implies a very small temperature rise in the fuel and clad of less than 2.2 ºC before the reactor control system shuts down the reactor.

Table 4.9. RIA of a 2.3 $ ramp in 500 ms (initial power = 80 kW; natural convection).

Core Description	Peak Fuel Centerline Temp. (°C)	Peak Clad Temp. (°C)	Peak Power (kW)	Trip	Time Step (s)
HEU, Fresh	56.1	56.0	148.70	Period	1.E-5
HEU, Burned	55.6	55.6	148.67	Period	1.E-5
LEU, Fresh	56.0	55.9	149.65	Period	1.E-5
LEU, Burned	55.5	55.4	149.69	Period	1.E-5

4.4 Concluding Remarks

1. It is shown that, with both period and power trips functional, the reactor can be safely shut down from an RIA of 2.3 $ as a ramp over 500 ms, without suffering excessive temperatures or burnout, for cores containing either all-fresh HEU, burned HEU, all-fresh LEU, or burned LEU. The minimum burnout ratio was 4.48, for these cases. The peak temperature of clad and meat remained below 105 ºC in all cases. This is well below the aluminum clad softening temperature of 450 ºC in the MITR SAR.

2. It is shown that the reactor can be safely shut down from a slow-insertion RIA of 0.03 dk/k over 60 seconds, without suffering excessive temperatures or burnout, for cores containing either all-fresh HEU, burned HEU, all-fresh LEU, or burned LEU. The minimum burnout ratio was 5.49, and the maximum temperature 107.2 ºC for the LEU cases.

3. It is shown that the reactor can be safely shut down from a 1 ms step-insertion RIA initiated at 5 W and essentially no flow (1 kg/s corresponding to a coolant velocity of 1 mm/s) of 1.5 $ without suffering excessive temperatures or burnout, for cores containing either all-fresh HEU, burned HEU, all-fresh LEU, or burned LEU.

4. Sensitivity studies of the effect of explicitly modeling fission product decay heat showed that the consequences are reduced because fission power is partially replaced by decay heat power. For example, if a 7-day prior operation period at full power is assumed for an HEU, fresh fuel RIA of 2.3$ in 500 ms, the peak power is reduced from 10.82 to 10.53 MW. The peak fuel temperature is reduced from 82.1 to 81.4 ºC. For a second example, if a 7-day prior operation period at full power is assumed for an HEU, fresh fuel RIA of 0.03 dk/k in 60 s, the peak power is unchanged at 8.04 MW. The peak fuel and clad temperatures are reduced by 0.002 ºC.

5. It is shown that the reactor can be safely shut down from a 2.3 $ ramp in 500 ms RIA initiated at 80 kW in steady-state natural convection flow without suffering excessive temperatures or burnout, for cores containing either all-fresh HEU, burned HEU, all-fresh LEU, or burned LEU.

5.0 LOSS OF PRIMARY COOLANT FLOW

The MITR is designed so that a low primary flow (less than 1800 gpm or higher) will automatically initiate a scram. There are two initiating events that can cause a loss of primary coolant flow accident. The first is a loss of off-site electrical power which will stop the primary pumps and scram the reactor by dropping all six shim blades simultaneously. This is a credible scenario. The second is a pump coast down accident that occurs because of primary pump power supply failures or malfunctions of the pump motors. This is not considered to be a credible accident because the probability for both pumps to fail at the same time is very small. The reactor will shut down automatically upon receiving a low primary coolant flow scram signal. The instrument delay time is less than one second. Analyses were performed for loss-of-flow accidents subject to the assumption that the power supply to both primary coolant pumps was interrupted at the same time.

For a given HEU or LEU core, a fuel plate stripe approach was used. Four stripes running lengthwise were used for each fuel plate in the core, with 18 axial nodes in each stripe. Neutronics calculations were made as discussed earlier to determine the power in each axial node of each stripe for each plate of each element in the core. Two cores, as listed in Table 5.1, were analyzed for the loss of flow accident. These all-fresh cores had the maximum power locations of a series of cores for which power shapes were calculated. This was done since the locations of maximum power are anticipated to yield limiting temperatures, although additional core states will be run in the next phase of analyses. All of these cores had finned fuel plates. The axial power shapes for these cores are shown in Figure 5.1.

Table 5.1. MITR Cores Used for LOF Analysis.

Core	Elements	Fuel	Peak Stripe/Core Average Power
HEU Fresh	22	UAl_x	1.463
LEU Fresh	22	U-10Mo	1.730

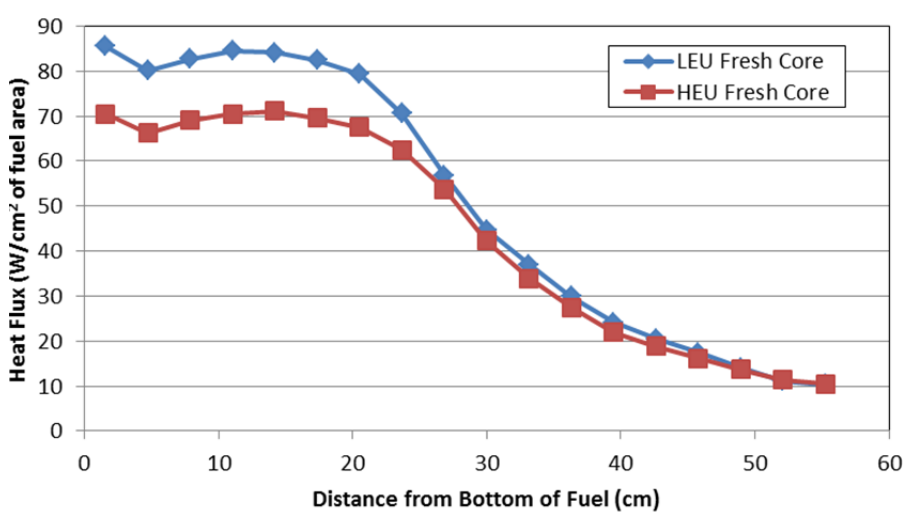

Figure 5.1. Axial Power Profiles of Cores for LOF Analysis.

5.1 RELAP5 Model

The RELAP5 Version 3.3 code was used for the LOF analysis. Most of the primary coolant loop was modeled. The model included the pumps, the downcomer inside the reactor vessel, the inlet plenum, the core, the outlet pool, the natural circulation valves, and the anti-siphon valves. The heat exchanger that removes the heat from the primary coolant loop was not explicitly included in the model, but the effect of the heat exchanger was included by holding the pump inlet temperature constant. Opening the natural circulation valves and the anti-siphon valves at low pump flow provided for a transition from forced flow to natural circulation during the LOF transient. For both HEU and LEU cases the thermal hydraulics model was identical except for the details of the core treatment.

Also in both HEU and LEU cases the locations of maximum power occurred in an end plate of an element facing the core housing inner wall. Therefore the core treatment included two peak channels. A peak interior channel represented half of the thickness of the peak stripe of the fuel plate plus half of the interior coolant in contact with the stripe. Zero heat flux boundaries were at the center of the fuel and the center of the coolant channel. A peak end channel represented the other half of the peak stripe of the fuel plate plus the end coolant in contact with the stripe plus the appropriate part of the core housing wall. Thus, the peak interior channel represented 1/8 of a fuel plate and 1/8 of an interior coolant channel. The peak end channel represented 1/8 of a fuel plate and 1/4 of an end coolant channel. An average interior channel was used to represent the rest of the interior channels, and an average end channel was used to represent the rest of the end channels. Also, an unheated bypass channel was used to represent coolant flow that did not go through the elements.

In the RELAP5 model all of the heat that the neutronics calculations predicted was conservatively assumed to be deposit in the fuel, clad and coolant was put in the fuel. RELAP5 contains an option to put a fraction of the heat directly into the coolant, but during boiling in the transient little heat would go directly into voided coolant channels.

The neutronics calculations indicated that a small fraction (4.5% for the LEU cases or 5.9% for the HEU case) of the power was deposited outside of the core elements. Some of this heat was deposited in the heavy water and graphite reflectors outside of the reactor tank, and some in the core structure and bypass flow. This heat was not included in the RELAP5 model.

Point kinetics was used by the code to calculate the impact of the scram reactivity on the transient power level. No reactivity feedback from heating the core during the transient was accounted for. Before the scram the feedback would be small, and after the rod insertion the scram reactivity would swamp the core feedback.

5.1.1 Conservative treatment of the peak channels

A number of conservative assumptions are used for the peak channels. First, as shown in Table 2.1, the coolant channel width in an element is somewhat larger than the width of the fuel meat. This extra coolant at the sides of the coolant is included in the average channels but ignored in the peak channels. Second, a flow disparity of 0.93 has been measured for the HEU core: the minimum element coolant flow rate is 93% of the average value. This flow disparity factor is applied to the peak channels by reducing the gap sizes. If the core pressure drop is proportional to the flow raised to the 1.75 power, then multiplying the gap size by 0.959 reduces the flow by 7%. Third, in the peak channels a two mil layer of oxide is added to the plate surfaces. Two mils is a reasonable upper limit for the oxide layer thickness. Because of the fins, adding two mils to a plate thickness reduces the effective gap size by 4 mils. In reality, the oxide layer would be formed by consuming a portion of the aluminum clad so that a two mil

oxide layer would have a somewhat reduced impact on the coolant flow area, but this is not accounted for in the model. Although there is a logical inconsistency in using a two mil oxide layer with a fresh core power shape the oxide was included because depleted cores will be analyzed in the next phase of work, and a bounding analysis was desirable. The objective of these preliminary analyses is to estimate the conditions and temperatures that fuel plates may experience in MITR. Although depleted cores have been found to have lower peak power the oxide will elevate temperatures during a LOF to some degree. For this reason including oxide layer on peak channels in fresh cores provides an upper estimate on the impacts of a LOF. Table 5.2 lists the impacts of these assumptions on the peak channel gap sizes.

Table 5.2. Coolant Gap Sizes (Fin Tip-Fin Tip, mil) Used for Peak Channels.

Fuel	Channel type	Channel assumed before reductions	Channel after reduction to account for flow disparity	Channel after reduction to account for flow disparity and oxide
HEU	Interior	78	74.4	66.4
HEU	End	44	42.0	36.0
LEU	Interior	72	68.6	60.6
LEU	End	38	36.2	30.2

Note: For an interior channel the effective gap is 10 mils more than tip-tip. For an end channel add 5 mil to get the effective gap.

Note that the before reducing the coolant gap the interior channel was set at the nominal specified value (78 mil for HEU and 72 mil for LEU). This reflects the nominal channel. As discussed in other work, the end channel is open on one side and so the dimension is defined by the surface adjacent to the element [1.4]. As shown in Tables 1-2 of that reference the end channel HEU dimension is 56.5 and LEU 50.5 mil nominally when the element is touching an adjacent surface. After tolerances including reactor structure, the end channels are treated very conservatively in these preliminary analyses starting at 44 and 38 mil for HEU and LEU respectively before disparity and oxide-related reduction. The various assumptions on channel reduction correspond to a value far below nominal and can be addressed in sensitivity studies in the next phase of accident analyses.

5.1.2 RELAP5 treatment of fins on the fuel plates

RELAP5 contains no explicit model for fins on fuel plates, but it is possible to adjust the RELAP5 input to account for fin effects. For the default surface heat transfer treatment (boundary type 1, 100 or 101) in RELAP5, the parameters that can be adjusted are:

S = plate surface area per axial node

and

D_{ht} = thermal hydraulic diameter, defined as 4 A_c/P_{erh} or 4 times coolant flow area divided by the heated perimeter.

For the friction pressure drop, the parameters that can be adjusted are:

D_h = hydraulic diameter, defined as 4 A_c/P_{erw} or 4 times coolant flow area divided by the wetted perimeter.

and

s_f = laminar shape factor.

Note that even though the RELAP5 heat transfer and friction calculations are based on correlations for flow in a circular pipe, Version 3.3 of the code does not require any geometrical consistency in the input values for the above four parameters, so they can be adjusted to model other geometries.

5.1.2.1 Heat transfer

The product hS is to be matched, where

h = surface heat transfer coefficient.

Use the subscript r for RELAP5, the subscript o for the actual value and the superscript * for the ratio of RELAP5 to actual. Thus:

$$h_r S_r = h_o S_o \tag{5.1}$$

or

$$h^* S^* = 1$$

define

r_f = surface area with fins/surface area without fins.

For the HEU design or the current base case LEU design, $r_f = 2$ in the fined region. Note that in the current stripe-based analysis the unfueled regions of the fuel plates near the side plates are ignored.

5.1.2.1.1 Turbulent Flow

For turbulent flow the Carnavos correlation [5.1] gives:

$$h_o = 0.023\ Re^{0.8} F_c Pr^{0.4} k/D_{hto} \tag{5.2}$$

where

F_c = Carnavos factor

Pr = Prandtl number which is a function only of the coolant temperature

k = coolant thermal conductivity

$Re = D_{hto} w/(u A_c)$

u = coolant viscosity

w = coolant mass flow rate (kg/s)

Note that Carnavos does not address the difference between an interior channel heated on both sides and an edge channel heated on one side and unheated on the other. Section 4.3.2 of Reference [5.2] does address this question for un-finned channels. This section indicates that for water in turbulent flow the presence of the un-heated side has little impact on the heat transfer coefficient of the heated side other than the change in the value of the thermal hydraulic diameter.

For turbulent flow RELAP5 gives:

$$h_r = 0.023\ Re_r^{0.8} Pr^{0.4} k/D_{htr} \quad (5.3)$$

Dividing Eq. 5.3 by Eq. 5.2 gives:

$$h^* = 1/(D_{ht}^{*\,0.2}\ F_c) \quad (5.4)$$

Combining Eq. 5.4 with Eq. 5.1 gives:

$$1 = S^*/(\ D_{ht}^{*\,0.2}\ F_c)$$

or

$$S^* = D_{ht}^{*\,0.2}\ F_c \quad (5.5)$$

5.1.2.1.2 Laminar Flow

For laminar flow the fins should have little impact on the heat transfer, so the heat transfer area and the heat transfer coefficient should be un-finned values. The laminar Nusselt number used by RELAP5 is:

$$Nu_r = 4.36 \quad (5.6)$$

which is appropriate for flow in a circular pipe. For flow in a flat duct, Section 3.3.1 of Reference [5.2] gives:

$$Nu_o = 8.235 \quad (5.7)$$

for an interior channel heated equally on both sides.

For an end channel with a fuel plate on one side and an un-heated plate on the other, the results depend on the ratio of the heat fluxes on the two surfaces. For a quasi-steady-state condition with little heat flux to the un-heated plate, the fuel plate result is

$$Nu_o = 5.38 \quad (5.8)$$

For a transient situation in which the heat flux into the un-heated plate happens to equal the heat flux out of the fuel plate, the result is

$$Nu_o = 4.0 \quad (5.9)$$

for both plates. The situations relevant to Equations 8 and 9 span the range of likely heat flux ratios, so Eqn. 9 will be used for both end channel plates.

For laminar flow Eq. 5.1 becomes:

$$k\ Nu_o\ S_o\ /(r_f\ D_{hto}) = k\ Nu_r\ S_r\ /\ D_{htr}$$

or

$$S^*/\ D_{ht}^* = Nu_o\ /\ (Nu_r\ r_f\ ) \quad (5.10)$$

Combining Eq. 5.5 and Eq. 5.10 gives:

$$D_{ht}^{*}\ Nu_o / (Nu_r\ r_f) = D_{ht}^{*\,0.2}\ F_c$$

or

$$D_{ht}^{*} = (F_c\ Nu_r\ r_f / Nu_o)^{1.25} \qquad (5.11)$$

Table 5.3. Heat Transfer Parameters for Current Designs

Fins	r_f	Channel	Plate	F_c	D_{ht}^{*}	S^{*}	$r_f\ S^{*}$
yes	2	interior	fuel	.72	.712	.673	1.346
yes	2	end	fuel	.72	1.757	.806	1.612
yes	1	end	un-heated	1.	1.114	1.022	1.022
no	1	interior	fuel	1.	.452	.853	.853
no	1	end	fuel	1.	1.114	1.022	1.022
no	1	end	fuel	1.	1.114	1.022	1.022

The stripe width used in RELAP5 should be multiplied by $r_f\ S^{*}$, and the plate thermal conductivity and volumetric heat capacity (density x heat capacity) should be divided by the same factor.

5.1.2.2 Friction Pressure Drop

The quantity to be matched is:

$$f\ (L/Dh)\ (\rho\ v^2/2)$$

where

f = friction factor
L = channel length
Dh = hydraulic diameter
v = coolant velocity

5.1.2.2.1 Inner Channel

For turbulent flow Reference [5.3] gives

$$f_d = 0.575\ Re_s^{-0.25} \qquad (5.12)$$

where the Reynolds number is based on the actual coolant flow area but a smooth surface rather than fins. Relap5 uses:

$$f_r = 0.316\ Re_r^{-0.25}$$

so

$$0.316\ (Dhr\ w / u\ Ac)^{-0.25}\ (L / Dhr)\ (\rho\ v^2/2) = 0.575\ (Dhs\ w / u\ Ac)^{-0.25}\ (L / Dhs)\ (\rho\ v^2/2)$$

or

$$0.316 / Dhr^{1.25} = 0.575 / Dhs^{1.25}$$

Thus:

$$Dhr / Dhs = (0.316 / 0.575)^{0.8} = 0.619 \quad (5.13)$$

For laminar flow Reference [5.3] gives

$$f = 91/Re_s \quad (5.14)$$

whereas Relap5 includes a shape factor, s_f and uses:

$$f_r = 64 / (Re_r\ s_f)$$

Thus:

$$64\ (Dhr\ w / u\ Ac\ s_f)^{-1}\ (L / Dhr)\ (\rho\ v^2/2) = 91\ (Dhs\ w / u\ Ac)^{-1}\ (L / Dhs)\ (\rho\ v^2/2)$$

or

$$s_f = 64 / [\ 91\ (Dhr/Dhs)^2\ )] = 64 / [91 \times .619^2] = 1.836 \quad (5.15)$$

5.1.2.2.1 End Channel

For turbulent flow, the end channel poses a special problem, since there is a finned plate on one side and a smooth plate on the other side. This situation has probably not been measured, so an approximation must be used. The friction factor is:

$$f = .316\ Re_s^{-.25} \text{ with no fins} \quad (5.16a)$$

or

$$f = .575\ Re_s^{-.25} \text{ with fins on two sides} \quad (5.16b)$$

so a reasonable approximation for the end channel with fins on one side is:

$$f = [(.316 + .575)/2]\ Re_s^{-.25} \text{ or } f = .446\ Re_s^{-.25} \text{ with fins on one side} \quad (5.16c)$$

Thus:

$$0.316\ (Dhr\ w / u\ Ac)^{-0.25}\ (L / Dhr)\ (\rho\ v^2/2) = 0.446\ (Dhs\ w / u\ Ac)^{-0.25}\ (L / Dhs)\ (\rho\ v^2/2)$$

or

$$0.316 / Dhr^{1.25} = 0..446 / Dhs^{1.25}$$

Thus:

$$Dhr / Dhs = (0.316 / 0.446)^{0.8} = 0.759 \quad (5.17)$$

For laminar flow Eq. 5.15 again gives:

$$s_f = 64 / [\ 91\ (Dhr/Dhs)^2\ )]$$

with the use of Eq. 5.17 this becomes:

$$s_r = 64 / [91 \times .759^2] = 1.221 \quad (5.18)$$

5.2 Initial Conditions and Assumptions

The initial conditions and assumptions made in this analysis were as follows:

a) The steady-state equilibrium reactor power was 7.2 MW for the HEU case and 8.4 MW for the LEU cases. These values are near or at the LSSS power values.
b) The primary coolant flow was 1800 gpm (LSSS flow rate).
c) The primary coolant outlet temperature was 60 °C (LSSS coolant outlet temperature).
d) The flow coast down curve is shown in Figure 5.2. This is measured for the upgraded primary heat exchanger, pumps, and coolant loop.
e) Because of the low flow reactor scram, the shim blades started to drop 1.0 seconds after the start of the pump coast down. Consistent with the Technical Specifications it was assumed that it would take one second for the shim blades to drop to 80% fully in position.
f) Because of low flow conditions the natural circulation valves and the anti-siphon valves opened 4 seconds after the start of the coast down.

The calculation started with a 300 second null transient with constant power and constant pump flow to establish initial steady-state conditions. The flow coast-down started at 300 seconds, the scram reactivity insertion started at 301 seconds, and the natural circulation and anti-siphon valves opened at 304 seconds.

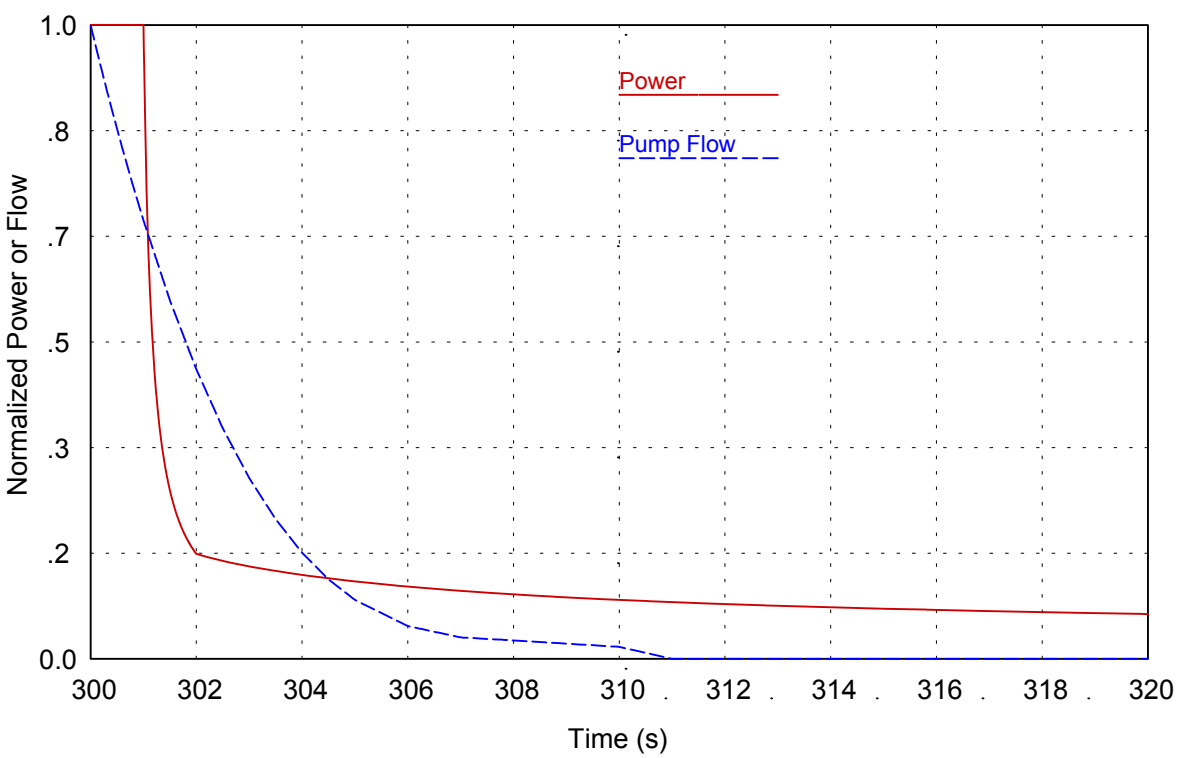

Figure 5.2. Calculated Power and Measured HEU Pump Coastdown Flow.

5.3 Results

Figures 5.3 to 5.5 show results from the HEU fresh core case. The pump trip at 300 seconds leads to a decrease in coolant flow and an increase in temperatures. At 301 seconds the scram reactivity insertion starts, and the power drops rapidly to decay heat levels. This leads to a rapid drop in temperatures. The temperatures bottom out and start to rise again near 304 seconds as the pump flow continues to drop. The opening of the natural circulation valves and the anti-siphon valves at 304 seconds leads to the development of natural circulation flow which limits further temperature increases.

It should be noted that the thermal resistance of the 2 mil (50.8 µm) oxide layer on the peak fuel plates is more significant than other regions of the plate. In steady state operation before the transient the temperature drop across the oxide is 17 ^{o}C at the peak node. In contrast the temperature drop across the rest of the plate to the center of the fuel is 4 ^{o}C, and the coolant film temperature drop is 47 ^{o}C.

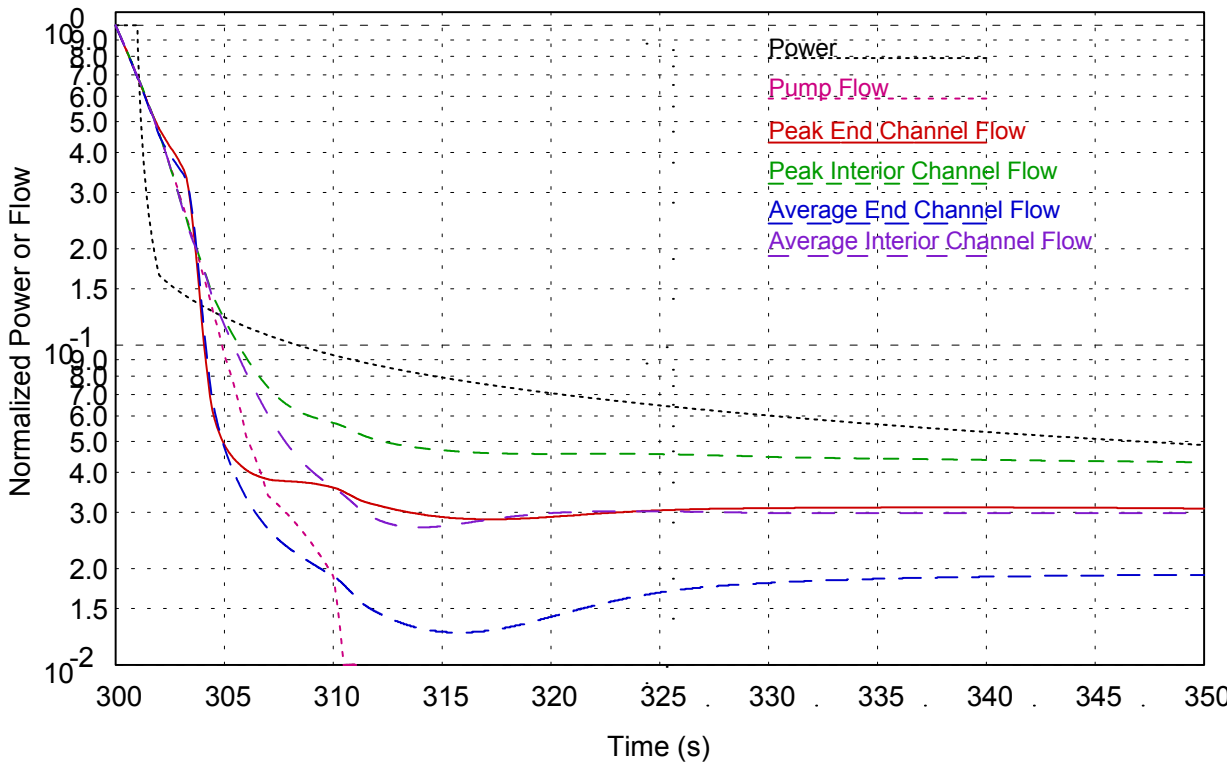

Figure 5.3. Power and Channel Flows for the Fresh HEU LOF.

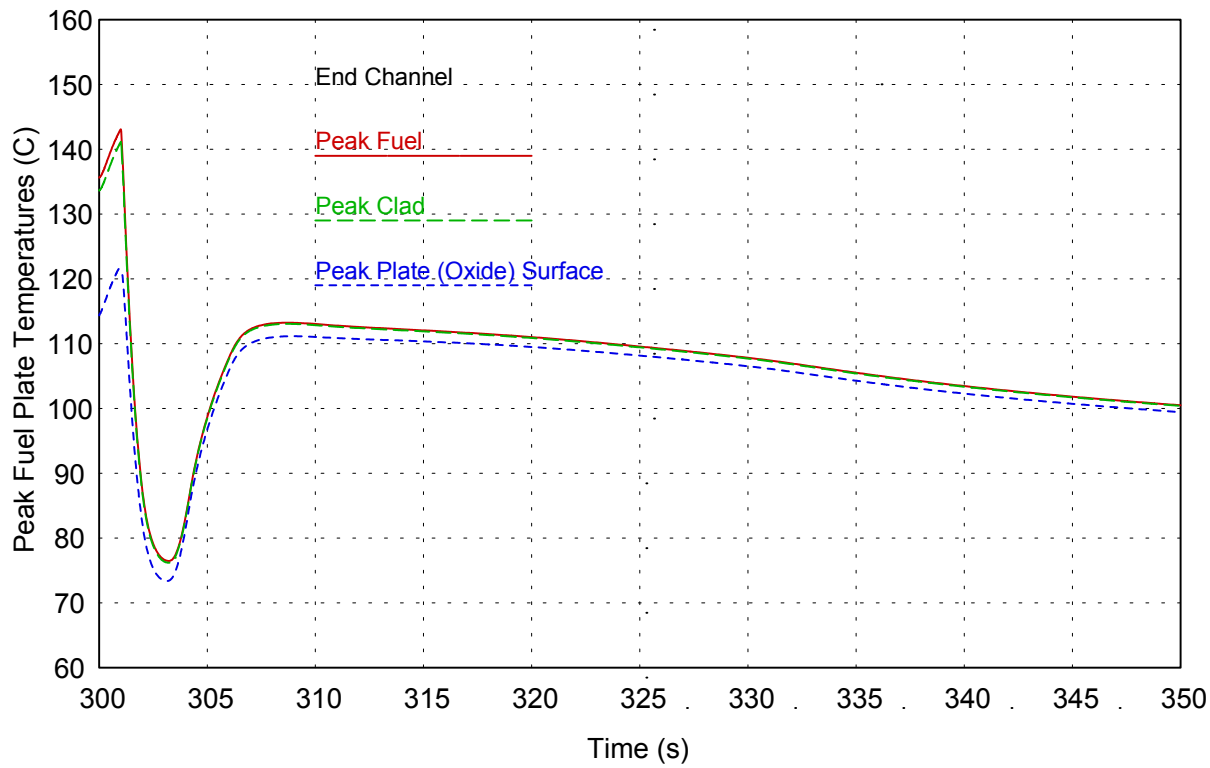

Figure 5.4. Peak End Channel Temperatures for the HEU Fresh Core LOF.

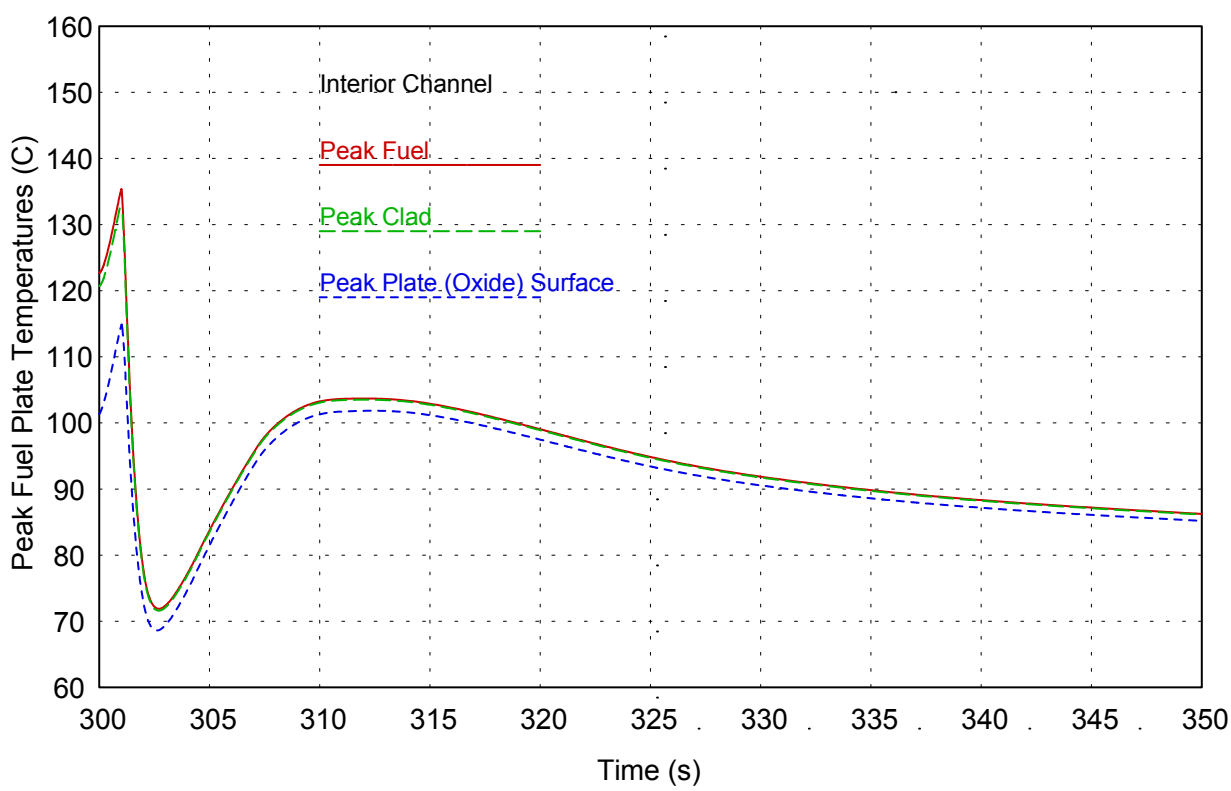

Figure 5.5. Peak Interior Channel Temperatures for the HEU Fresh Core LOF.

Figure 5.6 to Figure 5.10 show results for the fresh LEU LOF case. For the peak interior channel the LEU temperatures are only a few degrees hotter than the HEU results. On the other hand, the peak LEU end channel behavior is significantly different. In the peak end channel boiling causes a flow instability less than one second after the start of the pump coast-down. This leads to a rapid increase in steam pressure and the expulsion of the water from the whole axial length of the coolant channel, followed by depressurization as the steam blows out the ends of the channel. Depressurization leads to re-entry of liquid water from both ends and temporary cooling of the fuel plate. Figure 5.9 shows three such expulsion/re-entry events in about 0.6 seconds. The drop in power starting at 301 seconds soon leads to a temporary end to the violent boiling behavior, but Figures 5.6 and 5.8 show some milder boiling behavior at later times. Figure 5.10 does not indicate any such flow instability events in the peak interior channel.

It should be noted that for the fresh LEU case the peak end channel was already into extensive sub-cooled boiling (past ONB) during the steady state operation before the start of the flow coast-down, so it did not take long to reach flow instability after the pumps lost power. If the reactor had not been operating so close to the onset of flow instability before the start of the accident, the peak temperatures would have been significantly lower.

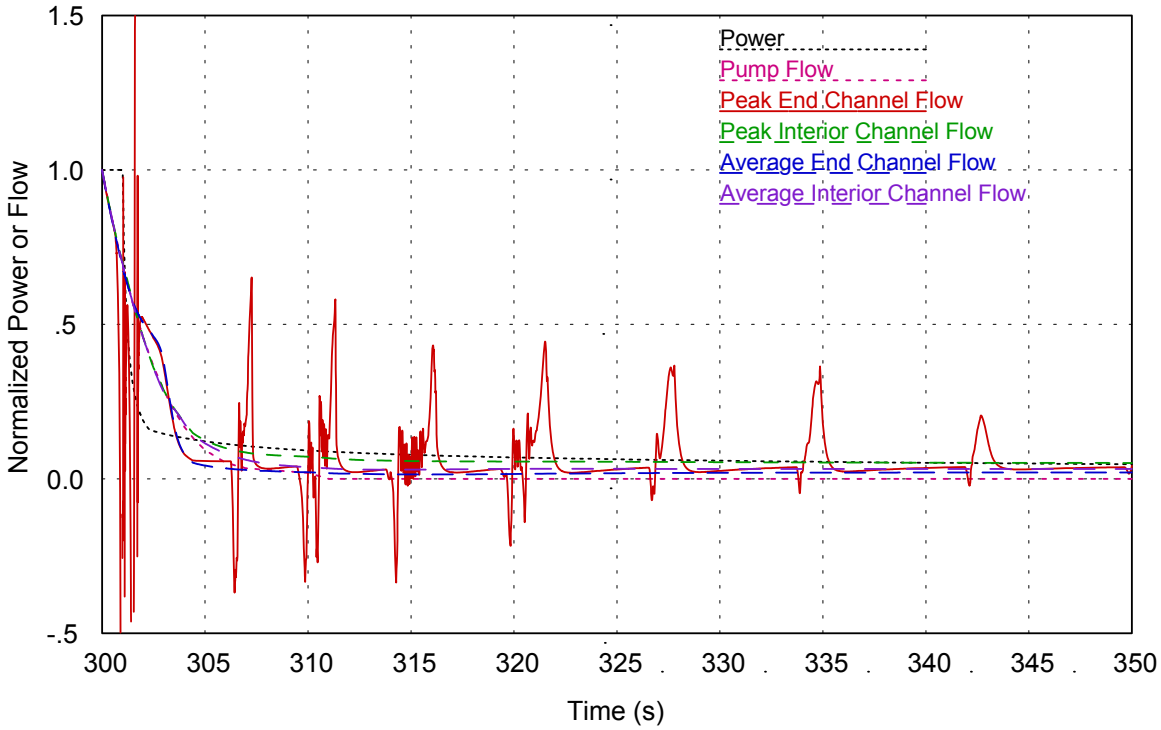

Figure 5.6. Power and Flows for the Fresh LEU LOF.

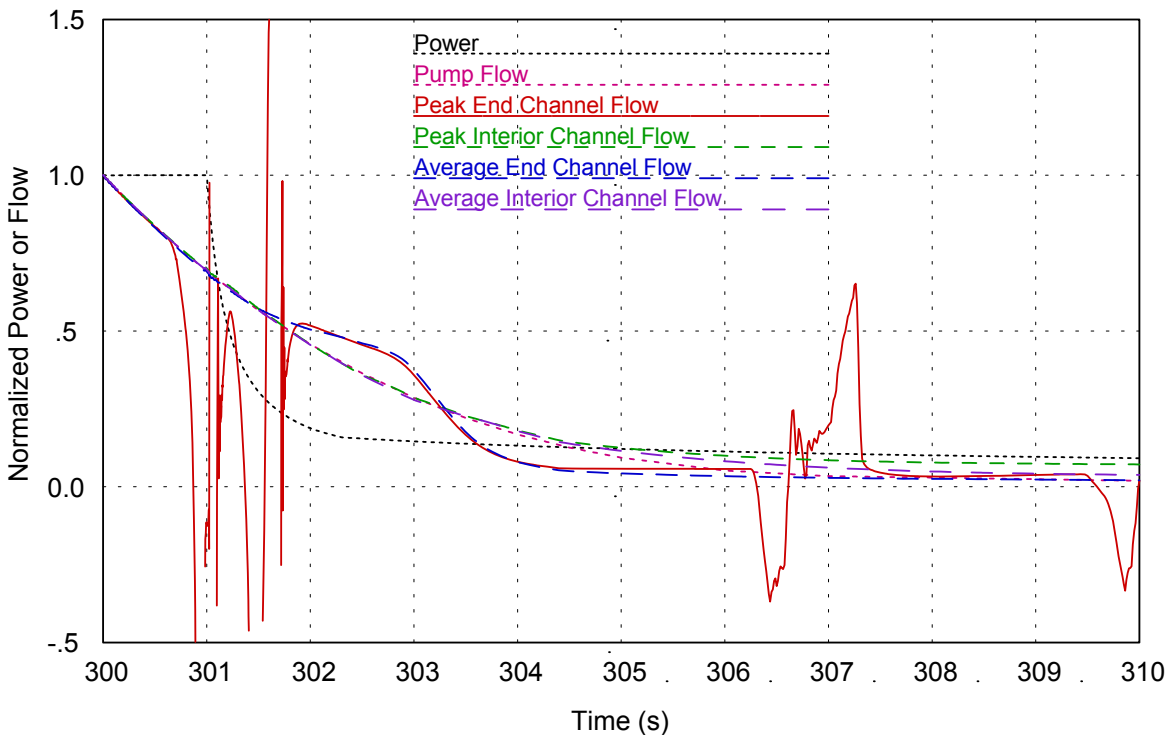

Figure 5.7. Expanded Time Scale for Fresh LEU LOF Power and Flows.

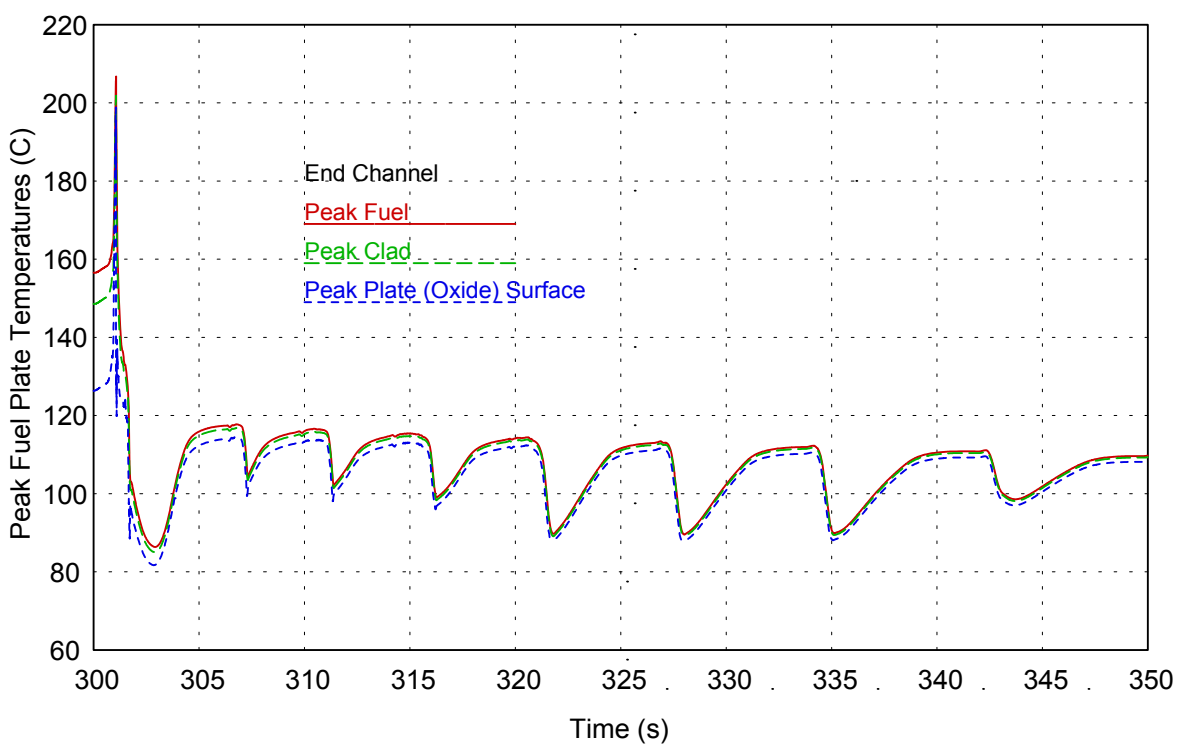

Figure 5.8. Peak Temperatures for the Fresh LEU LOF.

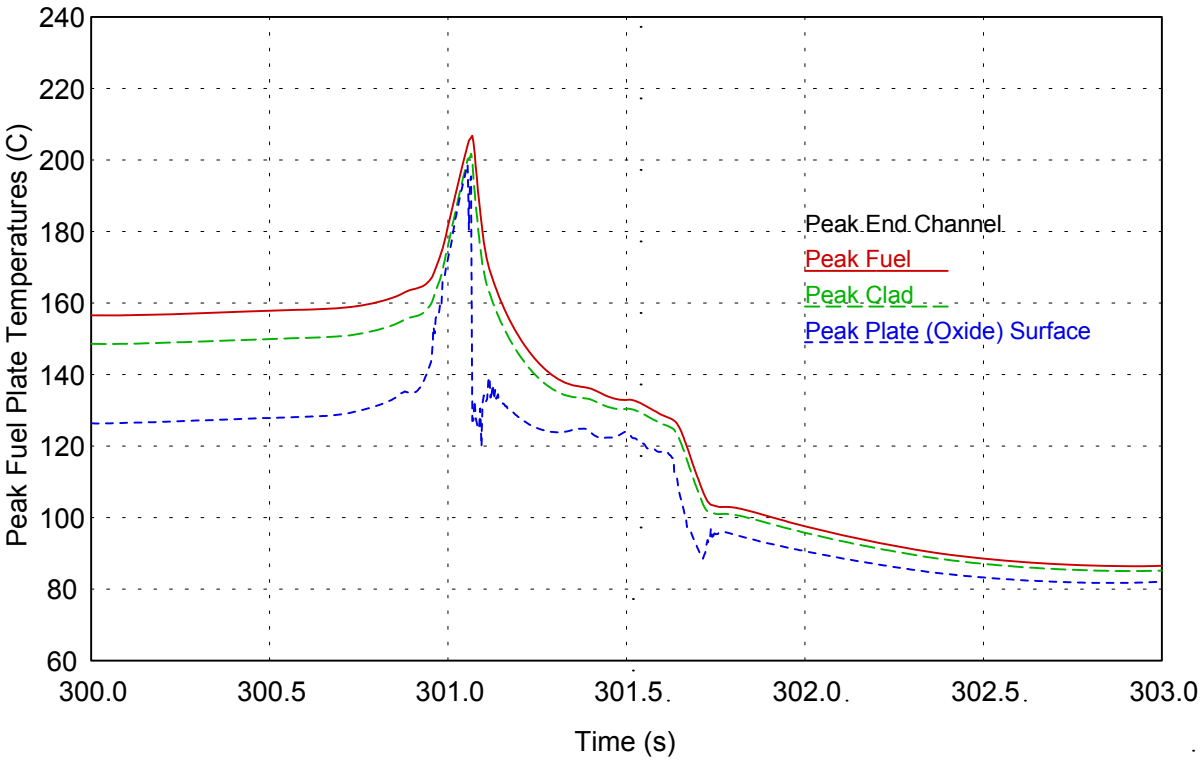

Figure 5.9. Expanded Time Scale for Peak End Channel Temperatures for Fresh LEU LOF.

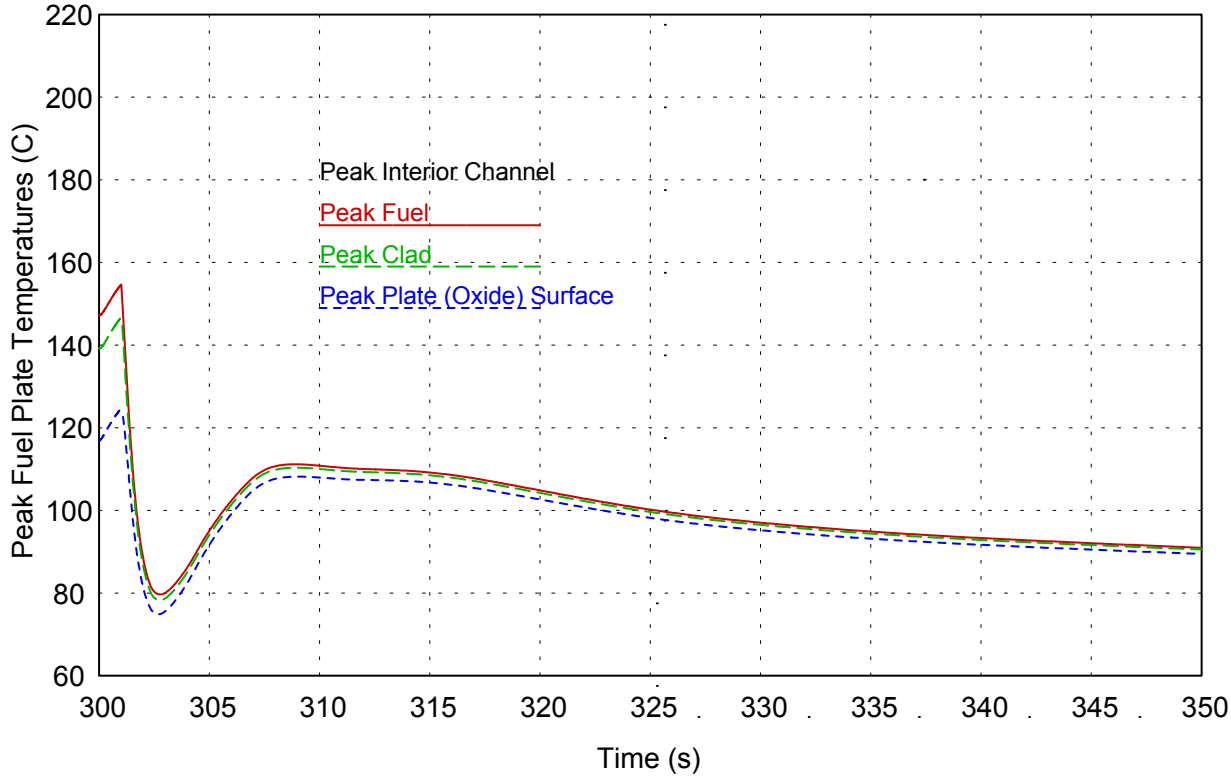

Figure 5.10, Peak Interior Channel Temperatures for Fresh LEU LOF.

Table 5.4 lists the peak temperatures for these cases in various regions of interest throughout the fuel plate from the peak temperature in the fuel center to the surface of the plate at the oxide-coolant interface. As a comparison to previous results, although power and geometry assumptions differed, the MITR HEU SAR [1.7] listed peak fuel temperature during a LOF as 118 °C.

Table 5.4. Peak Temperatures, °C, for the Loss-of-Flow Accident.

Case	Fuel center		Peak clad		Plate surface	
	Interior	End	Interior	End	Interior	End
HEU fresh	135.4	143.0	133.5	141.1	114.9	122.2
LEU fresh	154.6	206.7	146.7	201.7	124.7	198.8

5.4 Conclusions

The main conclusions from the LOF analyses are:

a) For the current LEU design the peak end channel is significantly more limiting than the peak LEU interior channel, and significantly more limiting than any HEU channel. Several factors in the model conservatisms and element design cause LEU end channels to be more limiting than other channels:
    1. LEU end channels are smaller than HEU end channels after incorporating 18 (thinner) plates to replace the 15-plate HEU design.
    2. The LEU end channel gap size is modeled to be 38 mil (before reductions to account for flow disparity and oxide). This is well below the nominal LEU end channel gap of 50.5 mil, and so is disadvantaged relative to the interior LEU channel modeled at nominal.
    3. An additional conservatism has been used for preliminary analysis by including a large oxide layer. This is done despite the cores being fresh in order to conservatively model the range of conditions and temperatures expected. LOF accidents with depleted will be modeled in the next phase of analyses and will study applying assumptions more applicable to the specific core state.

b) Even for the limiting LEU end channel design and with the conservative assumptions in the RELAP5 model, the peak fuel and clad temperatures are lower than 210 ^{o}C, which is significantly below the aluminum alloy softening temperature of 450 ^{o}C in the MITR SAR. This is also significantly below the expected blister temperature of monolithic UMo fuel, as discussed in Section 8.

6.0 HEAVY WATER AND LIGHT WATER MIXING

As introduced previously, the current MITR core is moderated and cooled by light water and has a heavy water reflector. Light water has both higher moderating power and absorption cross-section than heavy water does. In an under-moderated core with a hardened neutron energy spectrum such as the MITR, the effect of the high moderating power of light water outweighs its absorption effects, and, consequently, replacing coolant in the core with heavy water will result in a negative reactivity effect. However, in the exterior regions of the light water core tank, where the neutron energy spectrum is much softer, the absorption by light water outweighs the effect of its high moderating power so that replacing the light water with D_2O in the plenum above the fuel elements and along the walls and bottom of the core tank results in a momentary positive reactivity effect which is followed by a negative effect as the D_2O enters the core proper, i.e., the active region. Replacement of the heavy water in the reflector tank with light water will always result in a negative reactivity effect.

6.1 Leakage of Light Water into the Heavy Water Reflector

The effect of the leakage of light water into the heavy-water reflector is shown in Figure 6-1 for the HEU case. The newly obtained MCNP results (see Figure 6-1a) have been compared to the MITR Safety Analysis Report (SAR) [1.7] calculations carried out in the past (see Figure 6-1b).

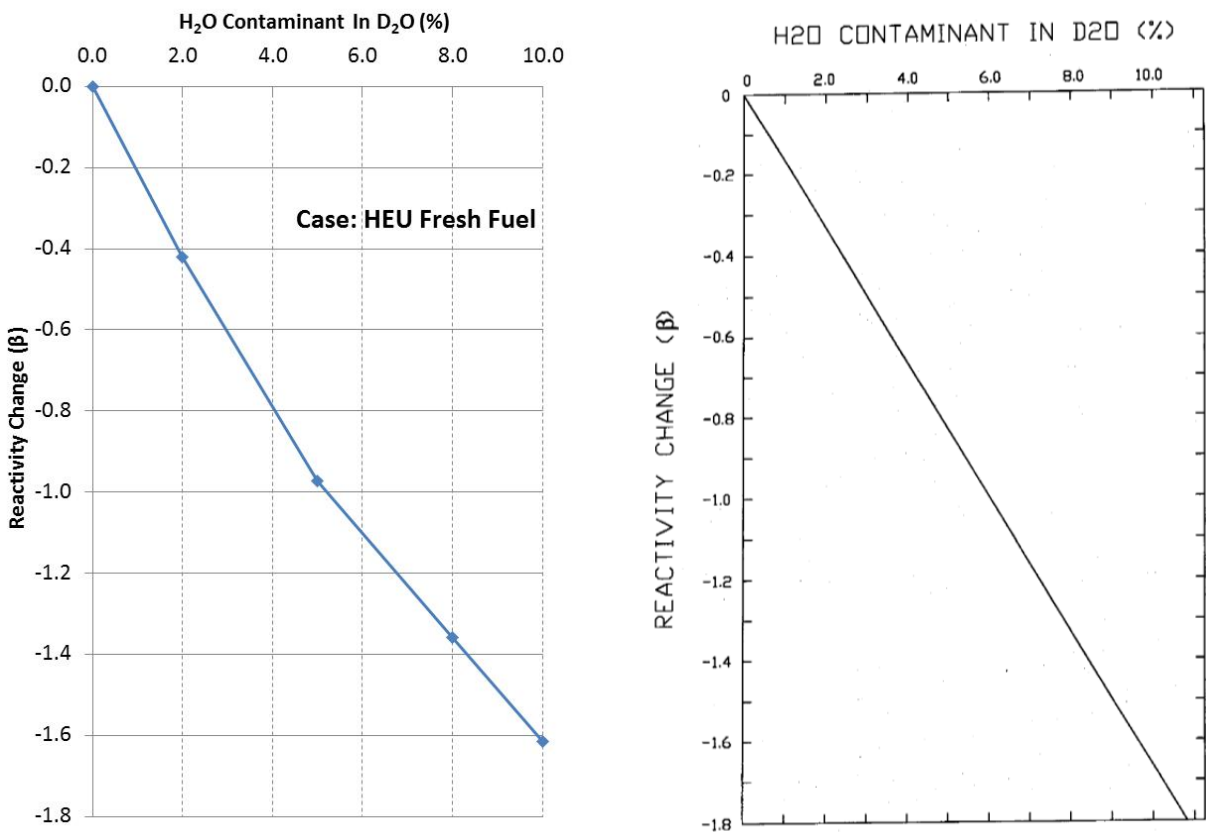

(a) **(b)**

Figure 6.1. Effect of light water leakage into the heavy water reflector (HEU case). (a) MCNP results and (b) from the SAR for the MITR.

As discussed above, the effect is a negative insertion of reactivity. With contamination of 10% light water in the heavy water reflector, an effect of ~ -1.6 β is predicted by MCNP and it agrees well to the SAR results in the past. In addition, this change is calculated to be approximately linearly dependent with the percentage of light water contamination. It should be noted that the calculation assumes homogeneous mixing of the light water with the heavy water in the reflector region. Local effects of H_2O leakage cannot, therefore, be inferred from this data.

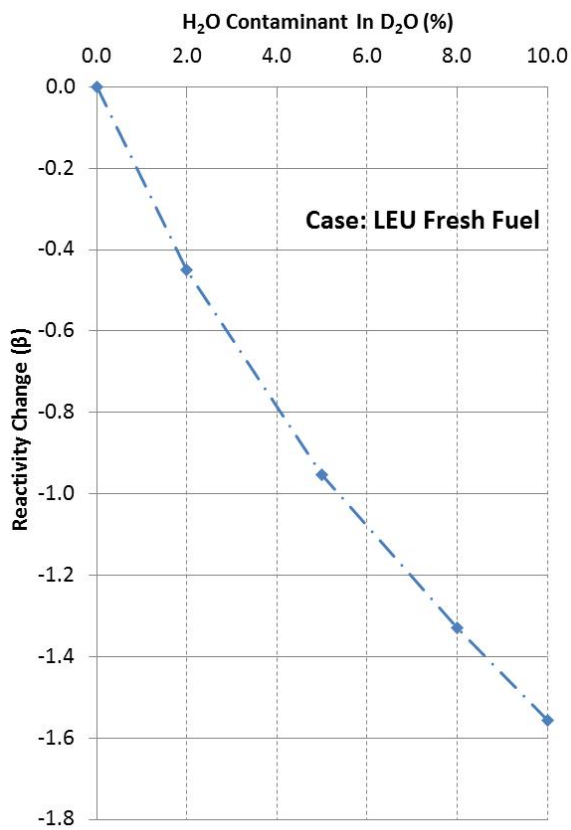

Figure 6.2. Effect of light water leakage into the heavy water reflector (LEU case).

In Figure 6.2, the equivalent set of heavy water reflector contamination results is presented for the LEU case. The curve is quite similar to the HEU curve in Figure 6.2: 1) negative reactivity insertion with linear correlation to the percentage of light water leakage and 2) magnitude of ~ -1.6 β in case of 10% mixing.

6.2 Leakage of Heavy Water into the Light Water System

The effects of heavy water leakage into the light water system are shown in Figure 6.3 for the HEU case. The newly obtained MCNP results (see Figure 6.3a) have been compared to the calculations carried out in the past (see Figure 6.3b). The leakage of pure, uncontaminated heavy water into either the light water above or below the core, or the light water annular space between the core and the sides of the core tank, results in a positive reactivity effect. On the other hand, leakage of heavy water into the light water of the core proper results in a strong negative reactivity effect. Similarly, progressively replacing the entire light water system with in-leaking heavy water will produce a strong negative reactivity effect.

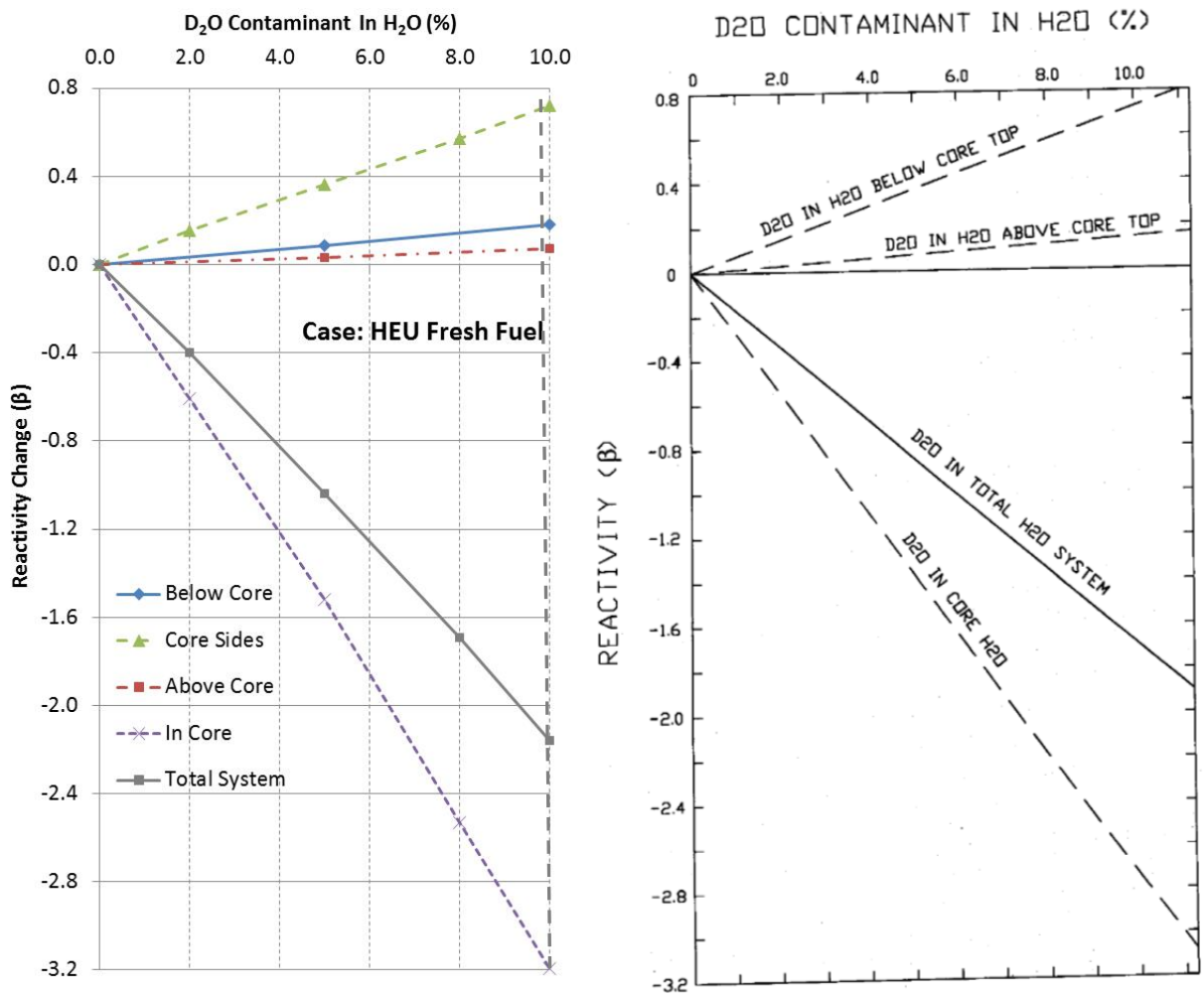

(a) **(b)**

Figure 6.3. Effect of heavy water leakage into the light water system (HEU case). (a) MCNP results and (b) from SAR for the MITR.

As can be seen, all of the calculated mixing cases are linearly correlated to the percentage of heavy water contamination. The two independent sets of results have generally good agreement for all of the scenarios studied. It is confirmed that the heavy water leakage into the non-active regions, namely, above or below the core, or the annular space between the core and the sides of the core tank, results in a positive reactivity effect. D_2O contamination of primary coolant below and above the "Core Top" has been analyzed in the SAR. On the other hand, significantly negative reactivity insertion can be found when the heavy water enters the core proper. Comparing to the SAR calculations in the past, a slight over-estimation for the negative reactivity effect can be found from the MCNP results.

Four points should be noted about the leakage of heavy water into the light water system. First, in the presented MCNP calculations, the "Below Core" and "Above Core" cases correspond to the mixing regions of the bottom (or top) end caps of the fuel element and the bottom (or top) grid plates. The "Core Sides" case refers to the primary H_2O in the down-comer and that around the shim blades. The latter reduces absorption rate of the reactivity control system due to the slightly hardened neutron spectrum and it is a somewhat important contributor to the positive reactivity effect. Second, the calculations were based on the assumption of homogeneous mixing of pure D_2O contaminant with light water in the various

regions listed in the figures. Hence, local effects, such as a small pinhole leak, are not directly inferable from the presented data. Third, the possibility of pure D_2O contaminating any region of the light-water system through a leak in the core tank is highly unlikely considering that the H_2O side of the system is the higher-pressure side. Lastly, the more likely occurrence is the situation in which the light water from the core tank leaks into the D_2O reflector region until the pressure is equalized on both sides of the core tank. At this point, it is quite possible to have the H_2O-contaminated heavy water diffuse, through the leak in the core tank, into the annular light water regions described above.

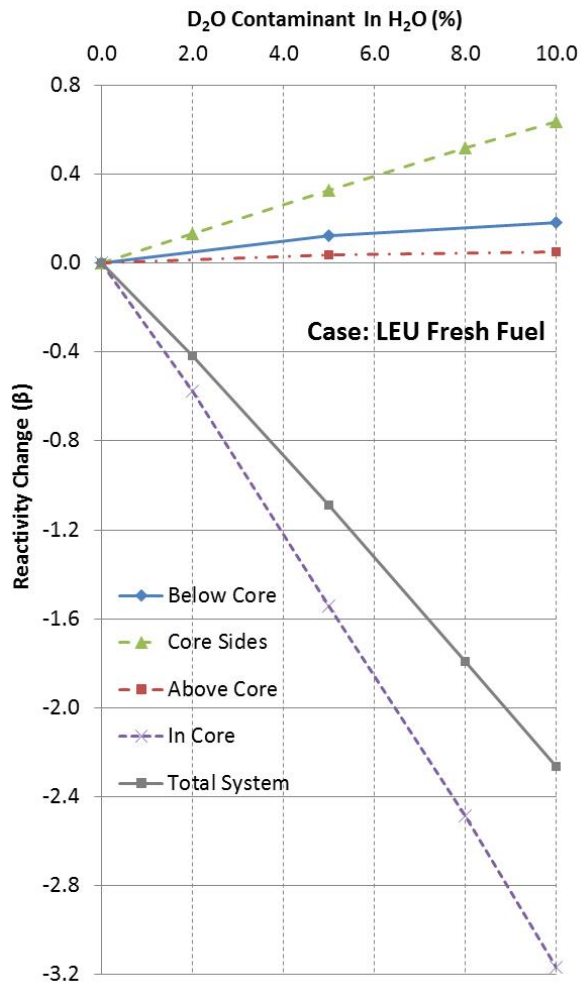

Figure 6.4. Effect of heavy water leakage into the light water system (LEU case).

In Figure 6.4, the equivalent set of the light water system contamination results is presented for the LEU case. Once again, the curves are very similar to the HEU ones in terms of both trend and magnitude: 1) positive reactivity insertion, when the heavy water leaks into either the light water above or below the core, or the light water annular space between the core and the sides of the core tank, and 2) significantly negative reactivity insertion, when heavy water mixes into the primary coolant of the core proper or progressively replaces the entire light water system.

7.0 MAXIMUM HYPOTHETICAL ACCIDENT

As discussed in the SAR, the maximum hypothetical accident (MHA) for the MITR is postulated to be a coolant flow blockage in the fuel element that contains the hottest fuel plate. In the HEU case, it is assumed that four fuel plates melt with the reactor operating at 6 MW. Plumer [7.1] analyzed the offsite dose consequences of the MHA with an 18 plate LEU fuel element whereby five fuel plates melt with the reactor operating at 7 MW. Two points external to the reactor containment building are chosen, one at 8 meters (the restricted area boundary) and one at 21 meters (the nearest point of public occupancy).

The Total Effective Dose Equivalent (TEDE) from the leakage, the Deep Dose Equivalent (DDE) from the direct gamma dose from the building, and the total TEDE results, are shown in Table 7.1. The release fractions used in this table are those for melted plates as in the MITR SAR, with the exception of the thyroid doses, which use LWR release fractions taken from NRC Regulatory Guide 1.195 [7.2]. These results show that the use of LEU fuel results in about a 22% increase in offsite doses. This is primarily due to the larger amount of material being released from an additional plate melting. The contribution of actinides from LEU fuel was found to be insignificant compared to the larger fission product source term.

It should be noted that the HEU values listed here are about 40% higher than those listed in the SAR. This is because additional isotopes that had not been previously included, such as Cs-138, were included in this model. In all cases, the total dose did not exceed the 0.5 rem limit of NUREG-1537. Additional details can be found in reference [7.1].

Table 7.1 MHA Dose results.

Fuel Type	HEU	LEU
Nominal Power (MW)	6	7
Leakage TEDE at 8 m (rem)	0.015	0.018
Leakage TEDE at 21 m (rem)	0.015	0.018
Thyroid dose at 8 m (rem)	0.084	0.109
Thyroid dose at 21 m (rem)	0.083	0.109
Gamma DDE at 8 m (rem)	0.265	0.325
Gamma DDE at 21 m (rem)	0.346	0.421
Total TEDE at 8 m (rem)	0.281	0.344
Total TEDE at 21 m (rem)	0.361	0.440

8.0 SUMMARY OF PRELIMINARY ACCIDENT ANALYSES

Safety analyses of the MITR core fueled with a monolithic alloy of uranium and 10 wt% molybdenum (U-10Mo) have been previously been conducted to establish the steady-state safety basis of the reactor. The thermal-hydraulic analyses of the reactor have required detailed power distributions and geometrical considerations in order to identify regions of interest for safety analyses. In order to understand the impacts of accident and transient scenarios in a core fueled with an LEU U-10Mo element, a set of preliminary accident analyses have been performed. NUREG-1537 guidelines postulate nine classes of accident-initiating scenarios. The preliminary analyses include evaluation of those which have been the most challenging to fuel integrity including reactivity insertion accidents, and a loss of flow accident.

Accidents resulting from the uncontrolled or unanticipated insertion of positive reactivity in the MITR core have been evaluated to assess the impact of fuel conversion on the reactor safety. First, positive reactivity insertion, based upon maximum reactivity limits given in the MITR Technical Specifications was considered. Second, a continuous ramp insertion of positive reactivity based on the continuous withdrawal of MITR's one shim control blade was considered. The exact mechanisms or events that could cause these reactivity insertions can vary, but could include an inadvertent rapid insertion or removal of an experiment.

For the most limiting HEU reactivity insertion accident, which was a 2.3 $ step insertion of reactivity in a fresh critical core at full power (6 MW), the peak HEU U-Alx fuel meat temperature is calculated to be 85.6 ºC. The LEU RIA ramp of 0.03 dk/k over 60 seconds from full power (7 MW) is the most limiting for the LEU fuel, resulting in a peak U-10Mo temperature of 107.2 ºC.

Accidents resulting from a loss of flow pump coast down were analyzed by a RELAP5 model in order to assess the impact of fuel conversion on the reactor safety. The peak HEU fuel temperature during the LOF is predicted to be 154.6 °C. For the LEU core, peak LEU fuel temperature during the LOF is predicted to be 206.7 °C. The HEU analyses were for 6 MW initial steady-state power, while the LEU analyses were for 7 MW initial steady-state power.

In all of these cases the fuel temperature is well below temperatures where fuel blisters have been experimentally observed. In UAl_x fuel blisters have been observed when irradiated fuel plates, at relevant fission densities, were placed in a furnace at or above 480 ºC [8.1]. Preliminary data with monolithic UMo alloy fuel has shown blisters at approximately 400 ºC for irradiated fuel [8.2]. These also show significant margin to the aluminum alloy clad softening temperature of 450 ºC in the MITR SAR.

The objective of these preliminary analyses was to determine the range of conditions and temperatures that the fuel, which is under development, should be expected to experience under off-normal and other transient scenarios. The preliminary results provided herein indicate acceptable thermal performance for the LEU core at 7 MW, and a reasonable comparison between the current and the MITR SAR results for the HEU core at 6 MW. Additionally, preliminary evaluation of heavy and light water mixing accidents scenarios and the MHA has been performed. The analyses reported herein represent the first phase of a two-phased effort to develop the complete Chapter 13 as a part of a complete LEU Conversion SAR.

These preliminary analyses considered limiting core power distributions, and focused on the thermal performance of the peak heat flux plates. Those plates were fresh for LOF, and both fresh and depleted for reactivity insertions. The LOF included conservatisms for both channel closure due to oxide and analysis of the more limiting end channels. RIA analysis did not assess the impact of either oxide or end channels which will be performed in subsequent Phase II analyses where the impact of channel gap closure and depletion will also be investigated. Phase II analyses will also assess the importance of fabrication tolerances and of uncertainties in fuel properties and initial conditions (flow, power, etc.).

Finally, additional improvement of the PARET/ANL and RELAP5 models will be considered in Phase II in order to reduce unnecessary conservatisms where appropriate. Any optimizations of element design to increase cladding thickness and other parameters for manufacturability and performance will also be incorporated in the subsequent phase of analyses.

ACKNOWLEDGEMENTS

The authors would like to thank U.S. Department of Energy, National Nuclear Security Administration Office of Global Threat Reduction (NA-21) for sponsoring this work. We gratefully acknowledge the expertise and knowledge of the engineering staff at both MIT and Argonne who contributed to this work. Particular recognition is due to Nick Horelik of MIT who lead recent developments in the MCODE fuel management simulations. Earl Feldman, Benoit Dionne and John Stevens of Argonne contributed to many discussions during the course of this work, and their expertise is gratefully acknowledged.

REFERENCES

[1.1] E.H. Wilson, T.H. Newton, Jr., A. Bergeron, N. Horelik, and J.G. Stevens, "Comparison and Validation of HEU and LEU Modeling Results to HEU Experimental Benchmark Data for the Massachusetts Institute of Technology MITR Reactor," ANL/RERTR/TM-10-41, Argonne National Laboratory, December 2010.

[1.2] T.H. Newton, Jr., E.H. Wilson, A. Bergeron, N. Horelik, and J.G. Stevens, "Neutronic Analyses for HEU to LEU Fuel Conversion of the Massachusetts Institute of Technology MITR Reactor," ANL/RERTR/TM-10-40, Argonne National Laboratory December 2010.

[1.3] L. Hu, K. Chiang, E.H. Wilson, F.E. Dunn, T.H. Newton, Jr., and J.G. Stevens, "Thermal Hydraulic Limits Analysis for LEU Fuel Conversion of the MIT Reactor," MITNRL-12-01, Massachusetts Institute of Technology, March 2012.

[1.4] E.H. Wilson, N. Horelik, F.E. Dunn, T.H. Newton, Jr., L. Hu, and J.G. Stevens, "Power distributions in Fresh and Depleted LEU and HEU Cores of the MITR Reactor," ANL/RERTR/TM-12-3 Revision 0, Argonne National Laboratory, February 2012.

[1.5] T.H. Newton, Jr., Dissertation "Development of a Low Enrichment Uranium Core for the MIT Reactor," Massachusetts Institute of Technology, Cambridge, Massachusetts, 2006.

[1.6] L. Hu, T.H. Newton, E.H. Wilson, J.G. Stevens, "Preliminary Safety Analysis Report Methodologies and Scenarios for LEU Fuel Conversion of the MITR Reactor," MITNRL-11-01, MIT Nuclear Reactor Laboratory, Massachusetts Institute of Technology, Cambridge, Massachusetts, April 2011.

[1.7] "Safety Analysis Report for the MIT Research Reactor," MITNRL-11-02, MIT Nuclear Reactor Laboratory, Massachusetts Institute of Technology, Cambridge, Massachusetts, August 2011.

[1.8] "Guidelines for Preparing and Reviewing Applications for the Licensing of Non-Power Reactors, Standard Format and Content," NUREG-1537, Part 1, U.S. Nuclear Regulatory Commission, February 1996.

[3.1] E.E. Feldman, et. al., "Preliminary Accident Analyses for Conversion of the University of Missouri Research Reactor (MURR) from Highly-Enriched to Low-Enriched Uranium," ANL/GTRI/TM-13/7, Argonne National Laboratory, June 2013.

[3.2] J. K. Fink and L. Leibowitz, "Thermal conductivity of zirconium," Journal of Materials, 226 (1995) 44-50.

[3.3] J.C. Griess, et al, "Effect of Heat Flux on the Corrosion of Aluminum by Water. Part IV. Tests Relative to the Advanced Test Reactor and Correlation with Previous Results," ORNL-3541, Oak Ridge National Laboratory, 1961.

[3.4] B.S. Hemingway, R.A. Robie, and J.A. Apps, "Revised values for the thermodynamic properties of boehmite, AIO(OH), and related species and phases in the system AI-H-O," American Mineralogist 76 (1991) 445.

[3.5] J. E. Matos and J. L. Snelgrove, "Selected Thermal Properties and Uranium Density Relations for Alloy, Aluminide, Oxide, and Silicide Fuel," Research Reactor Core Conversion Guidebook, IAEATECDOC-643, Volume 4: Fuels Appendices I-1.1, IAEA, Vienna, Austria, 1992, pp. 13-29.

[3.6] D. E. Burkes, G. S. Mickum, and D. M. Wachs, "Thermophysical Properties of U-10Mo Alloy," INL/EXT-10-19373, Idaho National Laboratory, November 2010.

[3.7] K.L. Peddicord, M.E. Cunningham, and A. Tripathi, "Porosity Correction to Thermal Conductivity Based on Analytical Temperature Solutions," Trans. Am. Nuc. Soc. 28 (1978) 548.

[3.8] J.C. Maxwell, *Treatise on Electricity and Magnetism*, first ed., Clarendon Press, Oxford, 1873.

[3.9] A. Eucken, Forsch. Geb. Ing., B-3, Forschung Sheft 53 (1932) 6–21.

[3.10] D.A.G. Bruggeman, Annal. Phys. 24 (1935) 636.

[3.11] J. Rest, Y.S. Kim, G.L. Hofman, M.K. Meyer and S.L. Hayes, "U-Mo Fuels Handbook," ANL-09/31, Argonne National Laboratory, November 2009.

[3.12] Y.S. Kim, and G.L. Hofman, "Fission Product Induced Swelling of U-Mo Alloy Fuel," Journal of Nuclear Materials 419 (2011) 291-301.

[3.13] E.H. Wilson, T.H. Newton, Jr., L. Hu, and F.E. Dunn, "Irradiation Experiment Conceptual Design Parameters for MITR LEU U-Mo Fuel Conversion," ANL/GTRI/TM-13/6, Argonne National Laboratory, June 2013.

[3.14] Y.S. Kim, "Thermal Degradation of U-Mo Fuel Dispersion in Al Matrix during Irradiation," Trans. Am. Nuc. Soc. (2013).

[4.1] A. Sakurai, M. Shiotsu, K. Hata and K. Fukuda, "Transition phenomena from non-boiling regime to film boiling on a cylinder surface in highly subcooled and pressurized water due to increasing heat inputs", ASME Paper 95-WA/HT-17 (1995) 1 – 11.

[4.2] J. Park, K. Fukuda and Q. Liu, "Effects of surface conditions on transient pool boiling CHF in various liquids with different mechanisms depending on pressure and subcooling", JSME Int. Journal Series B 49 (2) (2006) 318 – 325.

[4.3] J.G. Crocker, and L.A. Stephan, Reactor Power Excursion Tests in the SPERT IV Facility, AEC Research and Development Report, IDO-17000, August 1964.

[5.1] T.C. Carnavos, "Heat Transfer Performance of Internally Finned Tubes in Turbulent Flow", Heat Transfer Engineering 1:4 (1980) 32-37.

[5.2] S. Kakac, R.K. Shah and W. Aung, Handbook of Single Phase Convective Heat Transfer, John Wiley and Sons, New York (1987).

[5.3] S. Wong, L. Hu and M. Kazimi, "New Friction Factor Correlations for the MIT Reactor Fuel Elements", 31st RERTR 2009 International Meeting on Reduced Enrichment for Research and Test Reactors, Beijing, China (November 1-5, 2009).

[7.1] K. Plumer, "Estimate of Radiation Release from the MIT Reactor with Low Enriched Uranium Fuel During Maximum Hypothetical Accident," M.S. thesis, Massachusetts Institute of Technology, June 2011.

[7.2] U.S. Nuclear Regulatory Commission, Regulatory Guide 1.195, "Methods and Assumptions for Evaluating Radiological Consequences of Design Basis Accidents at Light-Water Nuclear Power Reactors," 2003.

[8.1] J. M. Beeston, R. R. Hobbins, G. W. Gibson, and W. C. Francis, "Development and Irradiation of Uranium Aluminide Fuels in Test Reactors," Nuc. Tech., 49 (June 1980) , 136-149.

[8.2] F. Rice, et al., "GTRI Blister Anneal and Fission Product Testing," U.S. High Performance Research Reactor Working Group Meeting, Los Alamos, New Mexico, June 11-13, 2013.

Nuclear Engineering Division
Argonne National Laboratory
9700 South Cass Avenue, Bldg. 208
Argonne, IL 60439

www.anl.gov

Argonne National Laboratory is a U.S. Department of Energy
laboratory managed by UChicago Argonne, LLC